The human nephrin Y[1139]RSL motif is essential for podocyte foot process organization and slit diaphragm formation during glomerular development

Received for publication, March 5, 2019, and in revised form, May 16, 2019 Published, Papers in Press, May 31, 2019, DOI 10.1074/jbc.RA119.008235

Eugenel B. Espiritu[‡], Huajun Jiang[§1], Sophie Moreau-Marquis[¶], Mara Sullivan[‖], Kunimasa Yan[‡‡], Donna Beer Stolz[‖], Matthew G. Sampson[**], Neil A. Hukriede[‡], and Agnieszka Swiatecka-Urban[§2]

From the [‡]Department of Developmental Biology, University of Pittsburgh School of Medicine, Pittsburgh, Pennsylvania 15201, the [§]Department of Pediatrics, University of Pittsburgh School of Medicine, Pittsburgh, Pennsylvania 15224, the [¶]Department of Microbiology and Immunology, Geisel School of Medicine at Dartmouth, Hanover, New Hampshire 03755, the [‖]Department of Nephrology, UPMC Children's Hospital of Pittsburgh, University of Pittsburgh School of Medicine, Pittsburgh, Pennsylvania 15201, the [‡‡]Department of Pediatrics, Kyorin University School of Medicine, Mitaka, Tokyo 181-8611, Japan, and the [**]Department of Pediatrics-Nephrology University of Michigan Medical School, Ann Arbor, Michigan 48109

Edited by Paul E. Fraser

Nephrin is an immunoglobulin-type cell-adhesion molecule with a key role in the glomerular interpodocyte slit diaphragm. Mutations in the *nephrin* gene are associated with defects in the slit diaphragm, leading to early-onset nephrotic syndrome, typically resistant to treatment. Although the endocytic trafficking of nephrin is essential for the assembly of the slit diaphragm, nephrin's specific endocytic motifs remain unknown. To search for endocytic motifs, here we performed a multisequence alignment of nephrin and identified a canonical *YXXØ*-type motif, Y[1139]RSL, in the nephrin cytoplasmic tail, expressed only in primates. Using site-directed mutagenesis, various biochemical methods, single-plane illumination microscopy, a human podocyte line, and a human nephrin-expressing zebrafish model, we found that Y[1139]RSL is a novel endocytic motif and a structural element for clathrin-mediated nephrin endocytosis that functions as a phosphorylation-sensitive signal. We observed that Y[1139]RSL motif–mediated endocytosis helps to localize nephrin to specialized plasma membrane domains in podocytes and is essential for normal foot process organization into a functional slit diaphragm between neighboring foot processes in zebrafish. The importance of nephrin Y[1139]RSL for healthy podocyte development was supported by population-level analyses of genetic variations at this motif, revealing that such variations are very rare, suggesting that mutations in this motif have autosomal-recessive negative effects on kidney health. These findings expand our understanding of the mechanism underlying nephrin endocytosis and may lead to improved diagnostic tools or therapeutic strategies for managing early-onset, treatment-resistant nephrotic syndrome.

The family of Ig-type cell-adhesion molecules (CAMs)[3] plays a critical role in cell signaling (1, 2). Nephrin is a type 1 transmembrane protein and an IgCAM essential for the glomerular interpodocyte slit diaphragm formation and function. Mutations in the *nephrin* gene are associated with defects in the glomerular slit diaphragm leading to nephrotic syndrome (NS) (3–7). *Nephrin* is one of the four genes whose mutations are responsible for the majority of NS cases that present before the first birthday and are characteristically resistant to treatment (8).

Podocytes are highly differentiated epithelial cells that wrap around capillaries of the kidney glomerulus and form a visceral layer of the Bowman capsule. Their tertiary projections or foot processes connect via an intercellular junction called the slit diaphragm. Despite intense research efforts, the exact molecular composition of the slit diaphragm has not been completely elucidated (9). Podocytes can engage diverse components of the intercellular junctions, depending on the developmental stage (9, 10). During early development, podocytes are connected by the tight junction and gap junction proteins that are partially and gradually replaced by the neuronal junction components, nephrin, podocin, and Neph1, which eventually form a structure resembling to some extent a neuronal synapse. Nephrin plays a central role in the formation and maintenance of mechanical properties of the slit diaphragm and in the podocyte inside-out and outside-in signaling (11, 12). Although

This work was supported by National Institutes of Health Grants T32DK061296 (to E. B. E.) and P30DK06010 and 1S10RR019003-01 (to N. A. H.), American Heart Association Grant 15GRNT25700019 (to A. S. U.), and NephCure Kidney International Grant 2012-RFE-003 (to A. S. U.). The authors declare that they have no conflicts of interest with the contents of this article. The content is solely the responsibility of the authors and does not necessarily represent the official views of the National Institutes of Health.

This article contains Figs. S1–S4.

[1] Present address: Dept. of Nephrology, Union Hospital, Tongji Medical College, Huazhong University of Science and Technology, Wuhan 430022, China.

[2] To whom correspondence should be addressed: Dept. of Nephrology, UPMC Children's Hospital of Pittsburgh, Pittsburgh, PA 15201. Tel.: 412-692-6710; Fax: 412-692-8906; E-mail: asurban@pitt.edu.

[3] The abbreviations used are: CAM, cell adhesion molecule; NS, nephrotic syndrome; AP-2, assembly polypeptide-2; CCV, clathrin-coated vesicle; CCP, clathrin-coated pit; MO, morpholino; SPIM, single-plane illumination microscopy; TEM, transmission electron microscopy; dpf, days postfertilization; MUSCLE, multisequence alignment with high accuracy and high throughput; CD2AP, CD2-associated protein; WES, whole exome; WEG, whole genome; hs- and dr-, human and zebrafish, respectively; WCL, whole-cell lysate; BA, Buffer A; PM, plasma membrane.

nephrin endocytosis is critical during podocyte differentiation (13, 14), the specific endocytic motifs remain elusive.

The cytoplasmic tail of human nephrin contains the YRSL sequence, which conforms to a clathrin-dependent consensus endocytic motif of the Y*XX*Ø type. The Y^{1139}RSL sequence, encoded by exon 27 of the human *nephrin* gene, is expressed only in primates (Fig. S1). Its localization 52 amino acid residues downstream from the membrane-spanning domain and 100 residues upstream from the nephrin C terminus is compatible with a role in endocytosis (15). Examination of genetic variation at this motif in human cases and the population support the potential importance of Y^{1139}RSL in nephrin function. A c.C3418T nucleotide change, resulting in p.R^{1140}C has been implicated as causal for congenital NS (in compound heterozygosity) in one of the first reported patients and was found as a single allele in siblings with congenital NS (4, 16). From a population genetics perspective, the Y^{1139}RSL sequence is very important because variation at this motif is rare, if not absent. In reviewing the gnomAD database of ~122,000 whole exomes (WES) and ~15,000 whole genomes (WGS) (http://gnomad.broadinstitute.org/),[4] the c.C3418T change reported as pathogenic above is only present in 0.01% of the population, and variation in the position 1141 amino acid residue is only seen in 0.0008% of the population. Other nonsynonymous changes affecting p.R^{1140} (p.R^{1140}S and p.R^{1140}H) are rare, affecting ~0.1% of the population. Synonymous or nonsynonymous variation affecting residue 1139 or 1142 is not observed at all.

Data presented herein demonstrate that the Y^{1139}RSL motif functions as a phosphorylation-sensitive signal for clathrin-dependent nephrin endocytosis, essential for the slit diaphragm formation.

Results

Human nephrin interacts with members of the clathrin-dependent endocytic pathway and post-endocytic recycling compartments

First, we examined whether human nephrin interacts with clathrin and the plasma membrane–associated endocytic adaptor complex, the assembly polypeptide-2 (AP-2) (17). Immortalized human podocytes were transfected with the WT human nephrin (Nephrin-WT) plasmid because endogenous nephrin expression was below detection by biochemical assays (Fig. S2). Nephrin-WT co-immunoprecipitated with endogenous clathrin and the μ2 adaptin of AP-2 (Fig. 1*A*). Next, we examined whether the cell surface abundance of Nephrin-WT is controlled by the large GTPase dynamin-2 that releases cargo containing clathrin-coated vesicles (CCVs) into the cell interior by membrane fission at the neck of clathrin-coated pits (CCPs) (18, 19). The dominant-negative dynamin-2 mutant DynK44A that blocks scission of CCPs increased the plasma membrane abundance of Nephrin-WT, as shown by the cell surface biotinylation assay (Fig. 1*B*). These data indicate that nephrin is internalized by a clathrin-dependent mechanism. Immunoprecipitation experiments showed that Nephrin-WT interacts with the small GTPases Rab4 and Rab8 (Fig. 1*C*). Rab4 and Rab8 are involved in recycling of the cargo molecules from early endosomes to plasma membrane, polarized membrane traffic, and interactions with the actin cytoskeleton (20). Together, these data show that in human podocytes, Nephrin-WT is internalized by clathrin-mediated endocytosis followed by trafficking in specialized, actin-based recycling compartments.

Mutagenesis of Nephrin-Y^{1139} affects tyrosine phosphorylation and changes nephrin abundance in CCVs

Interactions of the μ2 subunit of AP-2 with the Y*XX*Ø motif in membrane proteins trigger the formation of CCPs (21). The state of tyrosine phosphorylation in Y*XX*Ø motifs serves as a sensor to determine whether a protein should remain at the cell surface or undergo internalization (1, 22). Specifically, tyrosine dephosphorylation facilitates endocytosis by enabling the interaction of Y*XX*Ø with the μ2 adaptin (23). By contrast, tyrosine phosphorylation inhibits endocytosis and helps retain a protein at the cell surface because phosphorylated tyrosine cannot interact with the μ2 adaptin. To determine whether the Nephrin-Y^{1139} can function as such a sensor, we mutated it to alanine (Nephrin-Y1139A) or phenylalanine (Nephrin-Y1139F). The Nephrin-Y^{1139}A substitution should disable Y^{1139}RSL as an endocytic motif, whereas the Y^{1139}F substitution should mimic a nonphosphorylated state of the tyrosine residue and facilitate endocytosis. First, tyrosine phosphorylation of the nephrin variants was examined by anti-phosphotyrosine antibody 4G10 in immunoprecipitation experiments. There have been nine tyrosine residues reported in the nephrin cytoplasmic C-terminal tail (12). Compared with Nephrin-WT, tyrosine phosphorylation was reduced by the Y^{1139}F or Y^{1139}A substitution, indicating that the Nephrin-Y^{1139} is phosphorylated and thus may function in the context of the Y^{1139}RSL sequence as a phosphorylation-dependent sensor (Fig. 1, *D* and *E*).

Next, to examine whether altering the Nephrin-Y^{1139} phosphorylation affects clathrin-dependent nephrin endocytosis, we followed the abundance of Nephrin-WT, Nephrin-Y^{1139}F, or Nephrin-Y^{1139}A in CCVs isolated by density gradient and differential centrifugation, a procedure validated in our previous publication (24). Purity of the CCV fraction was confirmed by enrichment of the clathrin-associated μ2 adaptin, exclusion of the coat protein caveolin-1 associated with clathrin-independent endocytosis, and exclusion of the cargo protein podocin associated with lipid-raft membrane domains (Fig. 2, *A* and *B*). Nephrin-WT was enriched in the CCV fraction and co-distributed with clathrin and μ2 adaptin (Fig. 2, *A* and *B*). Clathrin abundance in the CCVs in podocytes expressing different nephrin variants was similar, indicating comparable isolation efficiency of the CCV fraction (Fig. 2*C*). The CCV abundance of Nephrin-Y^{1139}F, mimicking the dephosphorylated tyrosine, was increased, compared with Nephrin-WT. The results indicate that the Y^{1139}F substitution enabled the Y^{1139}RSL sequence to facilitate clathrin-dependent nephrin endocytosis (Fig. 2, *D* and *E*). Moreover, the CCV abundance of Nephrin-Y^{1139}A, disabling the Y*XX*Ø motif, was decreased compared with Nephrin-WT, indicating that the Y^{1139}A substitution

[4] Please note that the JBC is not responsible for the long-term archiving and maintenance of this site or any other third party hosted site.

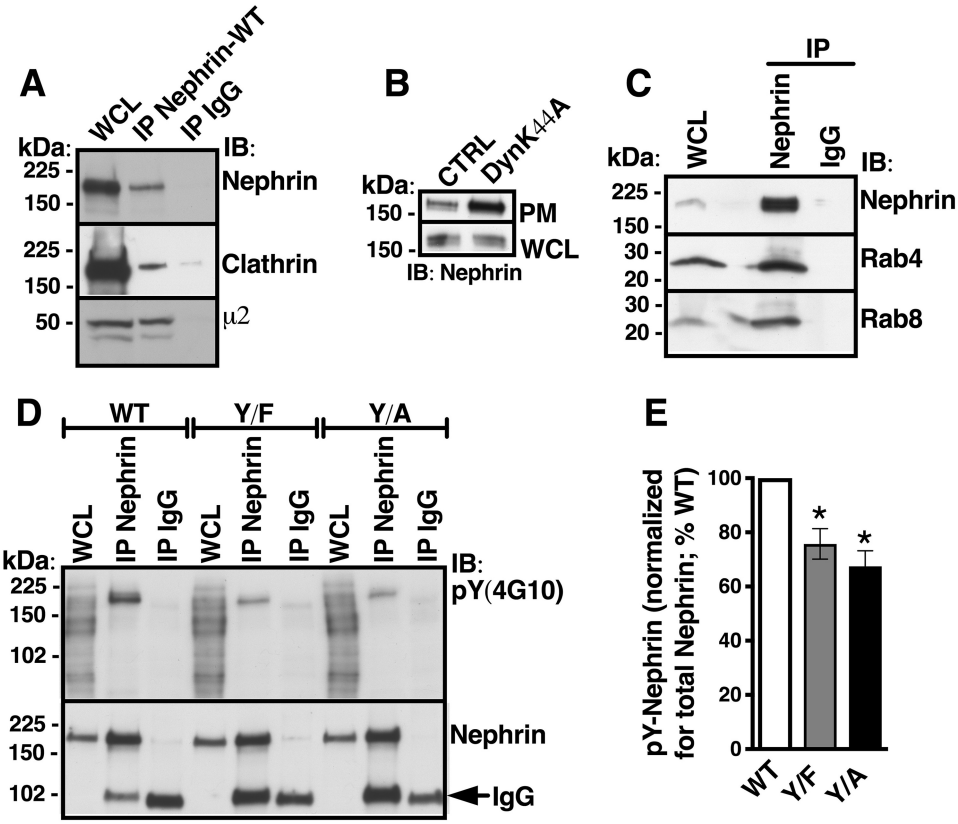

Figure 1. Human nephrin interacts with members of the clathrin-dependent endocytic pathway and post-endocytic recycling compartments, and Tyr^{1139} mutagenesis inhibits nephrin tyrosine phosphorylation. *A*, immunoblots (*IB*) demonstrating that Nephrin-WT co-immunoprecipitated with endogenous clathrin and the μ2 adaptin of the plasma membrane–associated clathrin adaptor complex, AP-2, in human podocytes. *B*, representative cell surface biotinylation experiments showing that DynK44A increased the abundance of Nephrin-WT specifically in the plasma membrane. Podocytes expressing Nephrin-WT were rapidly cooled to 4 °C to stop endocytic trafficking, and the plasma membrane (PM) proteins were labeled with membrane-impermeable EZ-Link^{TM} Sulfo-NHS-LC-Biotin, followed by cell lysis, isolation of biotinylated proteins with streptavidin beads, and elution from beads. The PM Nephrin-WT was detected in the biotinylated protein complexes, and the total cellular Nephrin-WT was detected in WCL by immunoblotting. *C*, co-IP experiments showing that Nephrin-WT interacts with the small GTPases, Rab4 and Rab8. Shown are immunoblots (*D*) and a summary (*E*) of IP experiments demonstrating contribution of the Tyr^{1139} residue to the total pool of phosphorylated tyrosine residues in Nephrin-WT. Nephrin-WT was immunoprecipitated from WCL with antibody 50A9 (*IP Nephrin-WT*) or nonspecific IgG control (*IP IgG*). Total Nephrin-WT, Nephrin-Y^{1139}F, and Nephrin-Y^{1139}A were detected with antibody N-20, and the tyrosine-phosphorylated form (*pY*) was detected with the phosphosite antibody 4G10 in the immunoprecipitated protein complexes. The immunoprecipitating IgG was nonspecifically visualized with anti-nephrin antibody N-20 (*arrow*). The Y^{1139}F (Y/F) substitution, a nonphosphorylated tyrosine mimic, and Y^{1139}A (Y/A) substitution in the Y^{1139}RSL motif reduced nephrin phosphorylation, demonstrating that nephrin is phosphorylated on the Tyr^{1139} site in human podocytes. The pY-Nephrin-WT, -Y/F, or -Y/A was normalized for the total immunoprecipitated nephrin, respectively, and expressed as a percentage of pY-Nephrin-WT. *A–C*, experiments were repeated three times in different cultures with similar results. *D* and *E*, *, $p < 0.05$ *versus* pY-Nephrin-WT (3 experiments/group). *Error bars*, S.E.

inactivated the Y^{1139}RSL sequence as an endocytic motif (Fig. 2, *D* and *E*). Because Nephrin-Y^{1139}A was still present in CCVs, the Y^{1139}RSL sequence is likely not the only clathrin-dependent endocytic motif in human nephrin. Nevertheless, these data demonstrate that the Y^{1139}RSL motif mediates clathrin-dependent nephrin endocytosis.

The Y^{1139}RSL motif modulates the steady-state abundance and stability of nephrin at the plasma membrane

We conducted cell surface biotinylation assays to determine effects of the Nephrin-Y^{1139} mutations on the steady-state plasma membrane abundance of nephrin. Whereas the three nephrin variants were detected at the plasma membrane, Nephrin-Y^{1139}F was less abundant and Nephrin-Y^{1139}A was more abundant, compared with Nephrin-WT (Fig. 3, *A* and *B*). Besides the role in clathrin-dependent endocytosis, *YXXØ* sequence may serve as a plasma membrane–targeting motif during protein biosynthetic processing (25). To confirm that the above differences in steady-state cell surface abundance resulted from altered endocytic trafficking, rather than different targeting to the cell surface, we examined effects of the Nephrin-Y^{1139} mutations on nephrin stability at the plasma membrane. Podocytes were treated with the inhibitor of translation cycloheximide (26). The plasma membrane half-life of Nephrin-Y^{1139}F (2.9 h) was decreased, and that of Nephrin-Y^{1139}A (7.4 h) was increased, compared with Nephrin-WT (4.5 h) (Fig. 4, *A* and *B*). The Nephrin-Y^{1139} mutagenesis affected specifically the plasma membrane and not the total cellular nephrin stability (Fig. 4, *A–C*). Our interpretation was that the nonphosphorylated tyrosine mimic, Y^{1139}F reduced the plasma membrane nephrin stability by accelerating nephrin endocytosis. By contrast, the Y^{1139}A substitution disabled the Y^{1139}RSL endocytic motifs and stabilized nephrin at the plasma membrane by inhibiting its endocytosis.

The Y^{1139}RSL motif affects podocyte migration

Podocytes exhibit contractile function (27). Increased podocyte motility is an important stress response leading to podo-

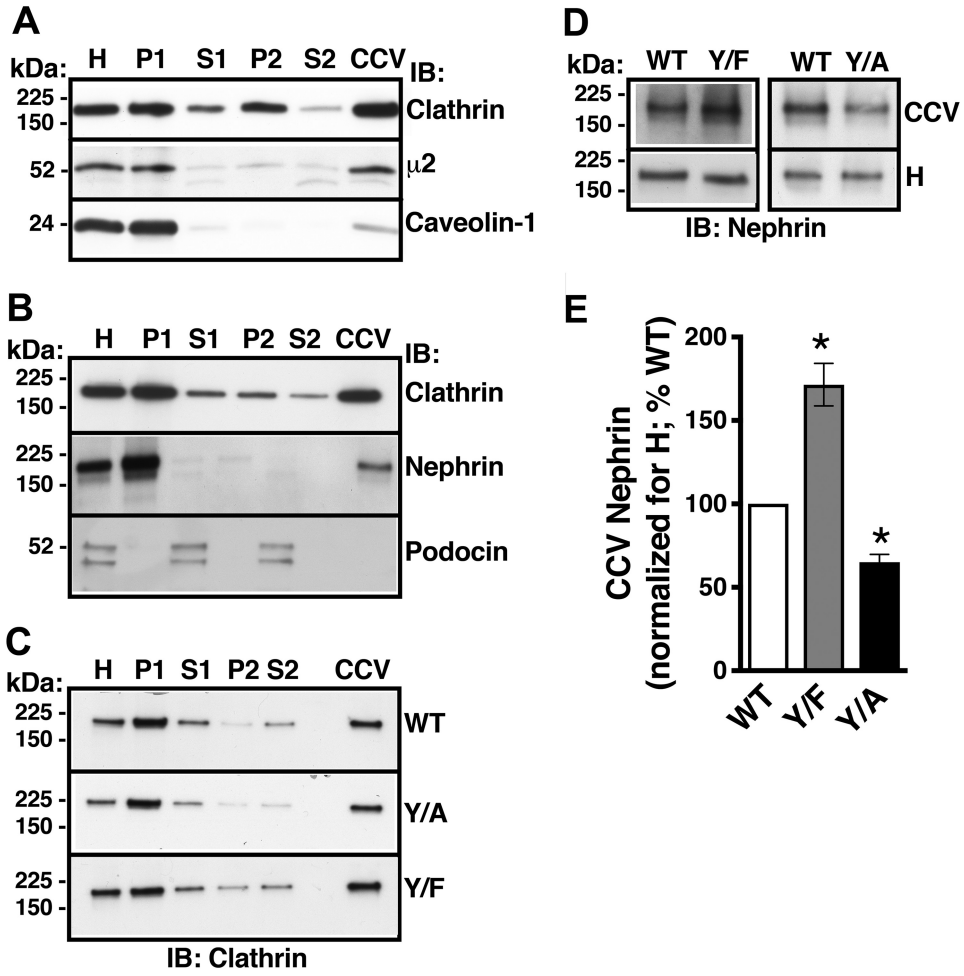

Figure 2. Mutagenesis of nephrin-Y^{1139} affects nephrin abundance in CCVs. Podocytes expressing Nephrin-WT, -Y^{1139}F, or -Y^{1139}A were first rapidly cooled to 4 °C to stop endocytic trafficking and synchronize the cell surface protein abundance, and subsequently, cells were rapidly warmed to 37 °C for 7.5 min to induce endocytic uptake of proteins into CCVs, followed by rapid cooling to 4 °C, and CCV isolation by density gradient and differential centrifugation. *A*, immunoblots (*IB*) demonstrating that the clathrin-associated μ2 adaptin and not the coat protein caveolin-1, associated with clathrin-independent endocytosis, co-distributed with clathrin. *H*, cellular homogenate; P_1, nuclear fraction; S_1, postnuclear supernatant; P_2, microsomal fraction; S_2, fraction depleted of microsomes. *B*, Nephrin-WT was targeted to CCVs. By contrast, the lipid raft–associated protein podocin was excluded from the CCV fraction. *C*, immunoblots confirming CCV isolation in podocytes expressing Nephrin-WT (*WT*), -Y^{1139}F (*Y/F*), or -Y^{1139}A (*Y/A*). Shown are immunoblots (*D*) and a summary of experiments (*E*) demonstrating that the CCV abundance of Nephrin-Y^{1139}F was increased and Nephrin-Y^{1139}A was decreased, compared with Nephrin-WT. The CCV abundance of WT, Y/F, and Y/A was normalized for the respective abundance in homogenates (*H*) and expressed as a percentage of WT. *, $p < 0.05$ *versus* Nephrin-WT. 3–5 experiments/group. *Error bars*, S.E.

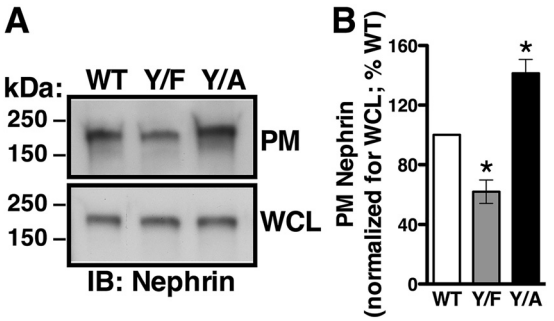

Figure 3. Cell surface biotinylation experiments demonstrating that the Y^{1139}RSL motif influences the steady-state plasma membrane nephrin abundance. Cell surface of podocytes expressing Nephrin-WT (*WT*), -Y^{1139}F (*Y/F*), or -Y^{1139}A (*Y/A*) was biotinylated with EZ-Link^{TM} Sulfo-NHS-LC-Biotin, and the PM nephrin was detected as described in the legend to Fig. 1*B*. The PM abundance of WT, Y/F, and Y/A was normalized for the respective abundance in WCL and expressed as a percentage of WT. Shown are immunoblots (*IB*) (*A*) and a summary of data (*B*) demonstrating that the steady-state PM abundance of Y/F was decreased and Y/A was increased compared with WT. *C*, *, $p < 0.05$ *versus* Nephrin-WT (3 experiments/group). *Error bars*, S.E.

cyte detachment (28–31). We performed a scratch assay to examine the role of the Y^{1139}RSL motif in podocyte motility. Podocytes expressing Nephrin-WT demonstrated baseline motility that was partially restricted by Nephrin-Y^{1139}F (Fig. 5). By contrast, Nephrin-Y^{1139}A increased podocyte migration by 2-fold compared with Nephrin-WT. The differences in number of cells in the scratch region did not result from differences in the cell-seeding density or cell division as determined by a comparable expression of nephrin variants or the housekeeping protein ezrin in podocytes expressing the nephrin variants (Fig. 5*C*). These data demonstrate that increased nephrin endocytosis, mediated by the Y^{1139}RSL motif, stabilizes podocytes, whereas inhibition of nephrin endocytosis induces podocyte migration. These results indicate that active nephrin turnover between the plasma membrane and intracellular compartments stabilizes podocytes and that the podocyte migratory responses are activated when nephrin becomes immobilized at the plasma membrane.

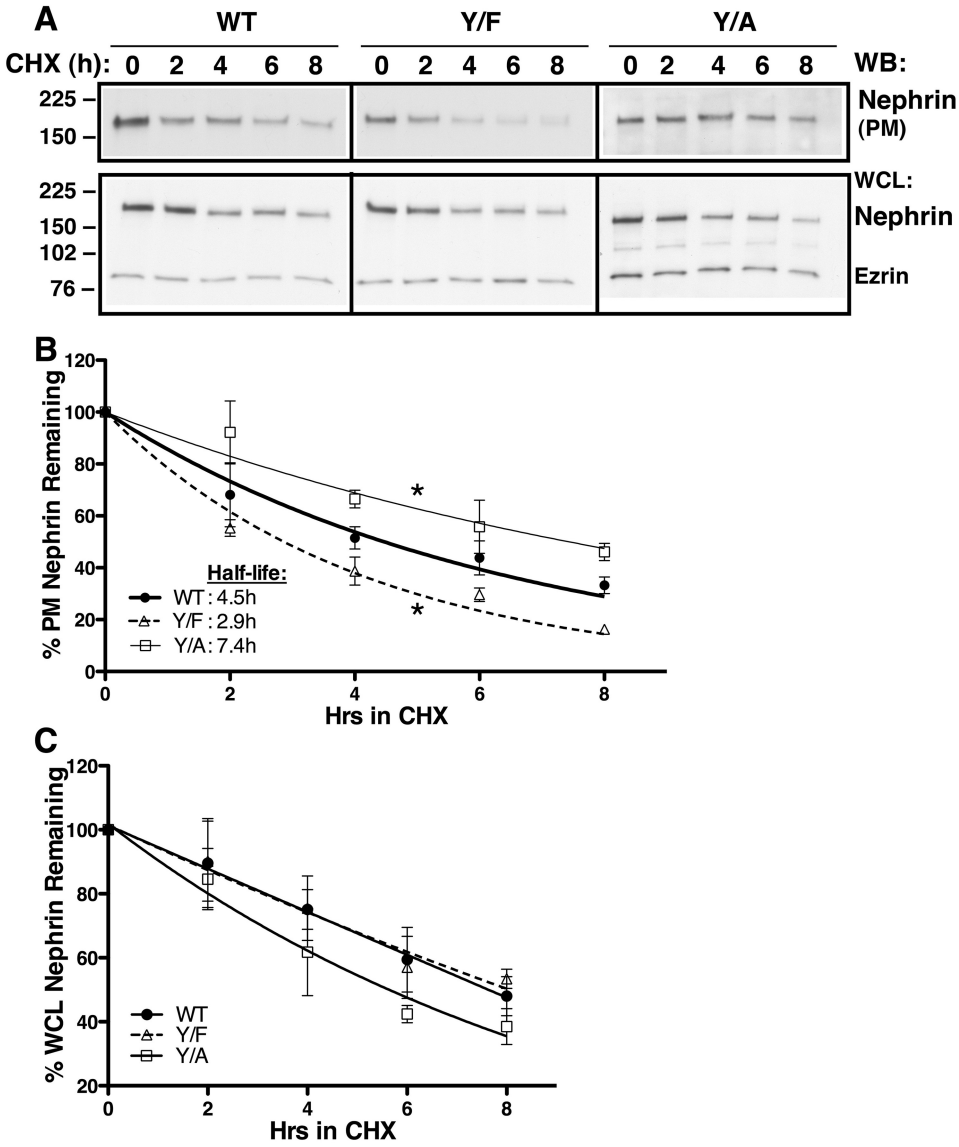

Figure 4. Cell surface biotinylation experiments demonstrating that the Y^{1139}RSL motif affects nephrin stability at the plasma membrane. Podocytes expressing Nephrin-WT (*WT*), -Y^{1139}F (*Y/F*), and -Y^{1139}A (*Y/A*) were cultured to confluence. Protein disappearance from the PM was monitored over time in the presence of 20 μg/ml cycloheximide (*CHX*) at 37 °C to inhibit protein translation. PM proteins were labeled with membrane-impermeable EZ-Link™ Sulfo-NHS-LC-Biotin. Ezrin expression in WCL was used as a loading control. The half-life was calculated using a one-way exponential decay model. Shown are immunoblots (*WB*) (*A*) and a summary of experiments (*B*) demonstrating that the plasma membrane half-life of Y/F (2.9 h) was shorter and that of Y/A (7.4 h) was longer, compared with WT (4.5 h). Nephrin stability in WCL was not affected by the amino acid substitutions at Tyr^{1139} (*C*). *, $p < 0.05$ *versus* WT (3–5 experiments/group). *Error bars*, S.E.

Modifications of the human nephrin-Y^{1139} alter the nephrin-rescuing ability in zebrafish morphants

To test the functional significance of the human Nephrin-Y^{1139}, we knocked down zebrafish nephrin and attempted to rescue with the human (hs)-Nephrin-WT, hs-Nephrin-Y^{1139}F, or hs-Nephrin-Y^{1139}A synthetic mRNA. Others have shown that human nephrin can rescue nephrin loss in zebrafish embryos and modifications to the human nephrin sequence alter the gene's rescuing abilities (32). Injection of validated nephrin morpholino (dr-Nephrin-MO) resulted in mis-splicing of zebrafish nephrin mRNA (Fig. S3). Embryos depleted of nephrin grown to 4 days postfertilization (dpf) exhibited pericardial and yolk sac edema as well as curvature of the body axis (Fig. 6*A*). In our rescue experiments, hs-Nephrin transcripts co-injected with dr-Nephrin-MO partially rescued nephrin mRNA expression with similar efficacy (Fig. S3, *C* and *D*). As shown by Fukuyo *et al.* (32), we were able to partially rescue the phenotypes, including edema associated with dr-Nephrin-MO, by co-injecting hs-Nephrin-WT with dr-Nephrin-MO (Fig. 6*B*). Similarly, co-injection of hs-Nephrin-Y^{1139}F significantly rescued dr-Nephrin-MO–mediated phenotypes. We did not observe rescue in embryos co-injected with Nephrin-Y^{1139}A and dr-Nephrin-MO when compared with embryos injected with the dr-Nephrin-MO alone.

To visualize the general organization of the glomerulus, we utilized transgenic zebrafish expressing enhanced GFP driven by the Wilms tumor 1a promoter (Tg(wt1a:eGFP) imaged by single-plane illumination microscopy (SPIM) (33). A pair of

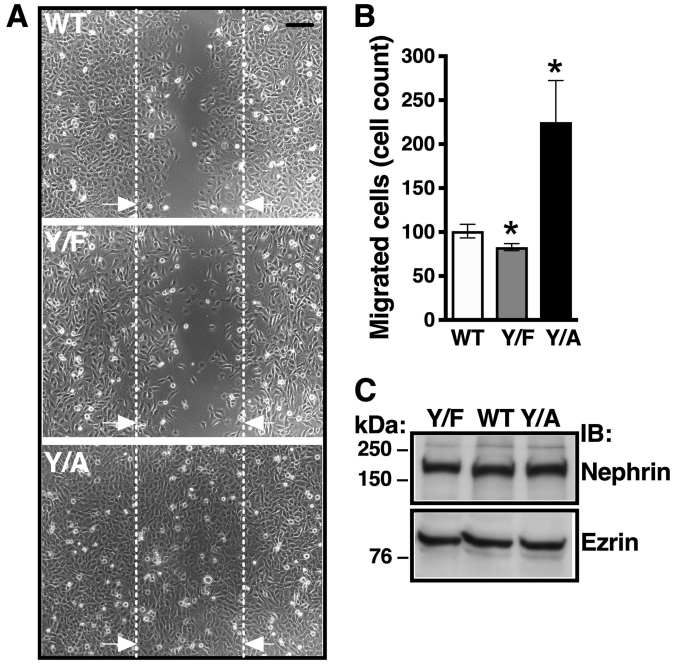

Figure 5. Cell migration assays demonstrating that Y^{1139}RSL influences podocyte migration. Podocytes stably expressing Nephrin-WT (*WT*), Nephrin-Y^{1139}F (*Y/F*), and Nephrin-Y^{1139}A (*Y/A*) were cultured to confluence on collagen I–coated 60-mm dishes. One scratch along the diameter of each dish was made using the P200 pipette tip, and reference points were made on the bottom of the dish. Cells were washed, and adherent podocytes were allowed to migrate into the scratch at 37 °C for up to 24 h, at which time podocytes expressing Nephrin-WT completely closed the gap created by the scratch. Thus, data were reported at the 8 h time point, at which cells were fixed with 2% paraformaldehyde. Images at ×10 magnification were obtained with a wide field microscope, and the cell nuclei were counted using the ImageJ software. The number of migrated cells was counted in four fields per condition in each experiment. Shown are wide field microscope images (*A*) and a summary of experiments (*B*) demonstrating that Y/F decreased and Y/A increased podocyte migration, compared with WT. *Interrupted lines* delineate the scratch reference points. *Arrows*, direction of cell migration. *Scale bar*, 300 μm. *C*, representative immunoblot showing similar expression of nephrin variants demonstrating similar cell seeding density. Ezrin was a loading control. *, $p < 0.05$ *versus* WT. 20–28 fields from 5–7 experiments/group. *Error bars*, S.E.

nephron primordia in zebrafish have fused at the midline by 2 dpf to both left and right pronephric tubules to serve a filtering function starting at 40 hpf (34–37), which we could see in all control animals. In uninjected animals and animals injected with control MO, the organization of the glomerulus showed no apparent gaps in the structure (Fig. 6, *C* and *D*). Conversely, nephrin morphants exhibited amorphous glomerular structures, specifically a decrease in size, failure of glomerular fusion, and cyst formation. These phenotypes were partially rescued with the co-injection of hs-Nephrin-WT or hs-Nephrin-Y^{1139}F in the dr-Nephrin-MO (Fig. 6, *C* and *D*). Whereas both partially rescued the amorphous glomeruli associated with dr-Nephrin-MO, morphants rescued with hs-Nephrin-Y^{1139}F fared significantly better than morphants rescued with hs-Nephrin-WT (Fig. 6*D*). Normal glomerular organization was observed in almost half of the edematous morphants rescued with hs-Nephrin-Y^{1139}F, whereas only a small fraction of edematous animals rescued with hs-Nephrin-WT and none injected with dr-Nephrin-MO alone had normal glomeruli (Fig. 6*E*). These data suggest that ultrastructural changes in the glomeruli, not observed by SPIM, could lead to edema formation in these animals. Morphants injected with Nephrin-Y^{1139}A failed to rescue, with a similar number of animals developing amorphous glomerular structure and edema, similar to animals injected with dr-Nephrin-MO alone (Fig. 6, *C–E*). The abnormal glomerular phenotypes appeared more severe for hs-Nephrin-Y^{1139}A and dr-Nephrin-MO, compared with hs-Nephrin-WT and hs-Nephrin-Y^{1139}F (Fig. 6, *C* and *D*). Although some morphants rescued with hs-Nephrin-WT or hs-Nephrin-Y^{1139}F did develop unfused glomeruli, the severity was lower (partial nonfusion) compared with morphants rescued with hs-Nephrin-Y^{1139}A or animals injected with dr-Nephrin-MO alone (Fig. 6, *C* and *D*).

To visualize the ultrastructure of the glomerulus, we utilized transmission EM (TEM). The podocyte foot processes and the slit diaphragm are formed and mature by 4 dpf (35). For all conditions, podocytes appeared to generate foot processes (Fig. 6*F*). All animals rescued with hs-Nephrin-WT (2 of 2) or hs-Nephrin-Y^{1139}F (3 of 3) appeared to have normal foot process organization. However, for a fraction of nephrin morphants (1 of 3) or animals rescued with hs-Nephrin-Y^{1139}A (2 of 6), we were unable to identify the presence of foot processes. In those we could identify, morphants and animals rescued with hs-Nephrin-Y^{1139}A exhibited amorphous foot process organization. This suggests that foot processes do form in animals rescued with hs-Nephrin-Y^{1139}A but do not organize into a functional slit diaphragm between neighboring podocytes; conversely, organization of foot processes can be rescued by hs-Nephrin-Y^{1139}F and hs-Nephrin-WT. Together, the above data demonstrate that the ability of human nephrin to rescue the phenotypes associated with nephrin depletion requires the residue Tyr^{1139} to be available for phosphorylation, and this residue is sufficient to improve nephrin activity in the formation of the slit diaphragm.

The human nephrin-Y^{1139}A has dominant-negative effects in the presence of dr-Nephrin

Finally, we examined effects of the human nephrin constructs in zebrafish embryos. Injection of hs-nephrin-WT and hs-nephrin-Y^{1138}F into blastomeres had a nearly undetectable effect on the development of animals. However, a large proportion of animals injected with hs-Nephrin-Y^{1139}A developed edema in a similar proportion to dr-Nephrin morphants alone and those co-injected with hs-Nephrin-Y^{1139}A (Fig. 7*A versus* Fig. 6*B*). Interestingly, animals injected with hs-Nephrin-Y^{1139}A alone exhibited abnormal glomerular structures, similar to those observed in the dr-Nephrin morphants co-injected with hs-Nephrin-Y^{1139}A, suggesting that the Y^{1139}A mutation had dominant-negative effects on the dr-Nephrin function and the glomerular development (Fig. 7*B versus* Fig. 6*D*). In reconciling the podocyte and zebrafish data, we propose that the dynamic nephrin turnover, maintained by the Y^{1139}RSL-dependent trafficking, is required for normal foot process organization and formation of the slit diaphragm during podocyte differentiation.

Discussion

We have shown that the Y^{1139}RSL motif is a structural element for clathrin-dependent nephrin endocytosis functioning

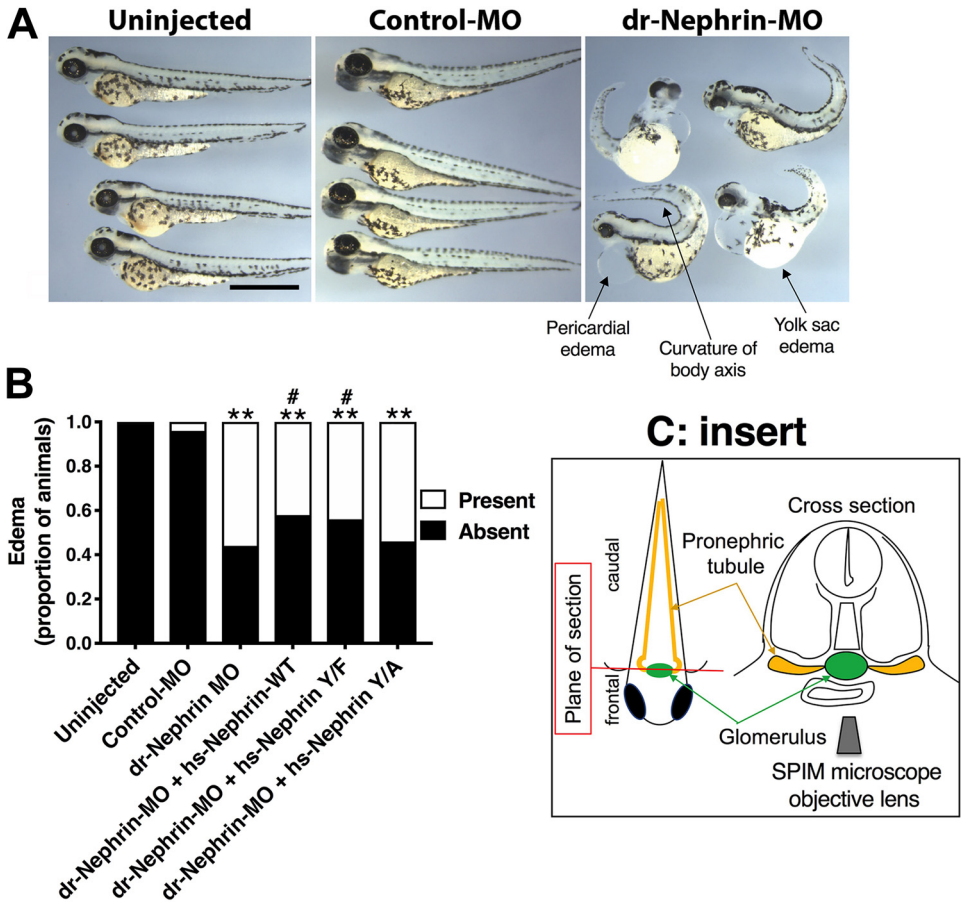

Figure 6. The human nephrin-Y^{1139}F is sufficient and required for human nephrin function and slit diaphragm formation in zebrafish embryos. Animals either uninjected or injected with Control-MO or dr-Nephrin-MO with or without co-injection of hs-Nephrin-WT, hs-Nephrin-Y^{1139}F (*Y/F*), or hs-Nephrin-Y^{1139}A (*Y/A*) were imaged in bright field at 4 dpf. *A*, representative images demonstrating normal phenotype of animals injected with Control-MO, compared with uninjected animals. Conversely, animals injected with dr-Nephrin-MO showed pericardial and yolk sac edema and curvature of body axis. *Scale bar*, 1 mm. *B*, proportion of animals that were phenotypically normal or had edema per denoted treatment. $n = 85–215$ animals/condition. *C*, fluorescence images of glomeruli obtained by a SPIM microscope in 4 dpf Tg(wt1a:GFP) animals injected with Control-MO or dr-Nephrin-MO alone or co-injected with dr-Nephrin-MO and hs-Nephrin-WT, Y/F, or Y/A. The *inset* shows the schematic plane of imaging. Shown are representative images of the patterns of glomerular organization and the number of animals in each treatment group. *Scale bar*, 200 μm. *D*, proportion of Tg(wt1a:GFP) animals with normal or abnormal glomerular patterns per denoted treatment. $n = 24–39$ animals/condition. Additionally, shown are the proportion of animals with specific patterns as subgroups in the abnormal glomerular organization group. *E*, proportion of animals grouped based on the presence or absence of edema with normal or abnormal glomerular organization per denoted treatment. $n = 24–39$ animals/condition. *F*, TEM images of the glomerular space of 4 dpf animals. All examined animals that were either uninjected or from the dr-Nephrin-MO + hs-Nephrin-WT group had no edema and showed normal ultrastructural organization of the glomerular ultrafiltration barrier, including the slit diaphragm seen as the *thin gray line* between neighboring foot processes. Two animals in the dr-Nephrin-MO group had edema, and one did not. We were unable to locate foot processes in the animal without edema, and shown is the ultrastructure of the edematous animal. For the dr-Nephrin-MO + hs-Nephrin-Y/F and dr-Nephrin-MO + hs-Nephrin-Y/A animals, one had edema and two were normal, and four had edema and two were normal, respectively. Animals with edema are shown for both groups. The *white arrows* show normal foot processes linked by a slit diaphragm. The *black arrows* show abnormal (effaced) foot processes that do not form a slit diaphragm. *Scale bar*, 500 nm; *glom*, glomerulus; *po*, podocyte cell body; *us*, urinary space; *gbm*, glomerular basement membrane; *fp*, foot process; *sd*, slit diaphragm; *ce*, capillary endothelium. *, $p < 0.05$; **, $p < 0.0001$ *versus* Control-MO. #, $p < 0.05$ *versus* dr-Nephrin-MO.

as a phosphorylation-sensitive signal. We propose that the Y^{1139}RSL-mediated endocytosis and post-endocytic trafficking maintain dynamic nephrin turnover and facilitate nephrin delivery to specialized membrane domains between neighboring foot processes, leading to organization into a functional slit diaphragm (Fig. 8).

Several lines of evidence support these conclusions. First, human nephrin co-immunoprecipitated with clathrin and AP-2, and residue Tyr^{1139} was phosphorylated in podocytes (Fig. 1). Second, the Y^{1139}F substitution, mimicking nonphosphorylated tyrosine, increased nephrin abundance in CCVs and reduced the steady-state abundance and stability of nephrin at the podocyte cell membrane (Figs. 2–4). Conversely, the Y^{1139}A substitution, disrupting the *YXXØ* endocytic motifs, had opposite effects. Our data showing significant decrease rather than complete blockade of Nephrin-Y^{1139}A entry into CCVs suggest the presence of additional endocytic motifs directing clathrin-dependent endocytosis of human nephrin (Fig. 2). Third, podocyte migration was restricted by Nephrin-Y^{1139}F and it was increased by Nephrin-Y^{1139}A, compared with Nephrin-WT (Fig. 5). These data support a view that the dynamic nephrin turnover rather than its immobilization at the cell membrane is important for the physiologic podocyte function. Consistent with this model, inhibition of endocytosis resulted in increased podocyte stress response. Fourth, hs-Nephrin-Y^{1139}F was superior to hs-Nephrin-WT in rescuing the phenotypes associated with nephrin depletion and defects in glomerular and foot process organization in zebrafish

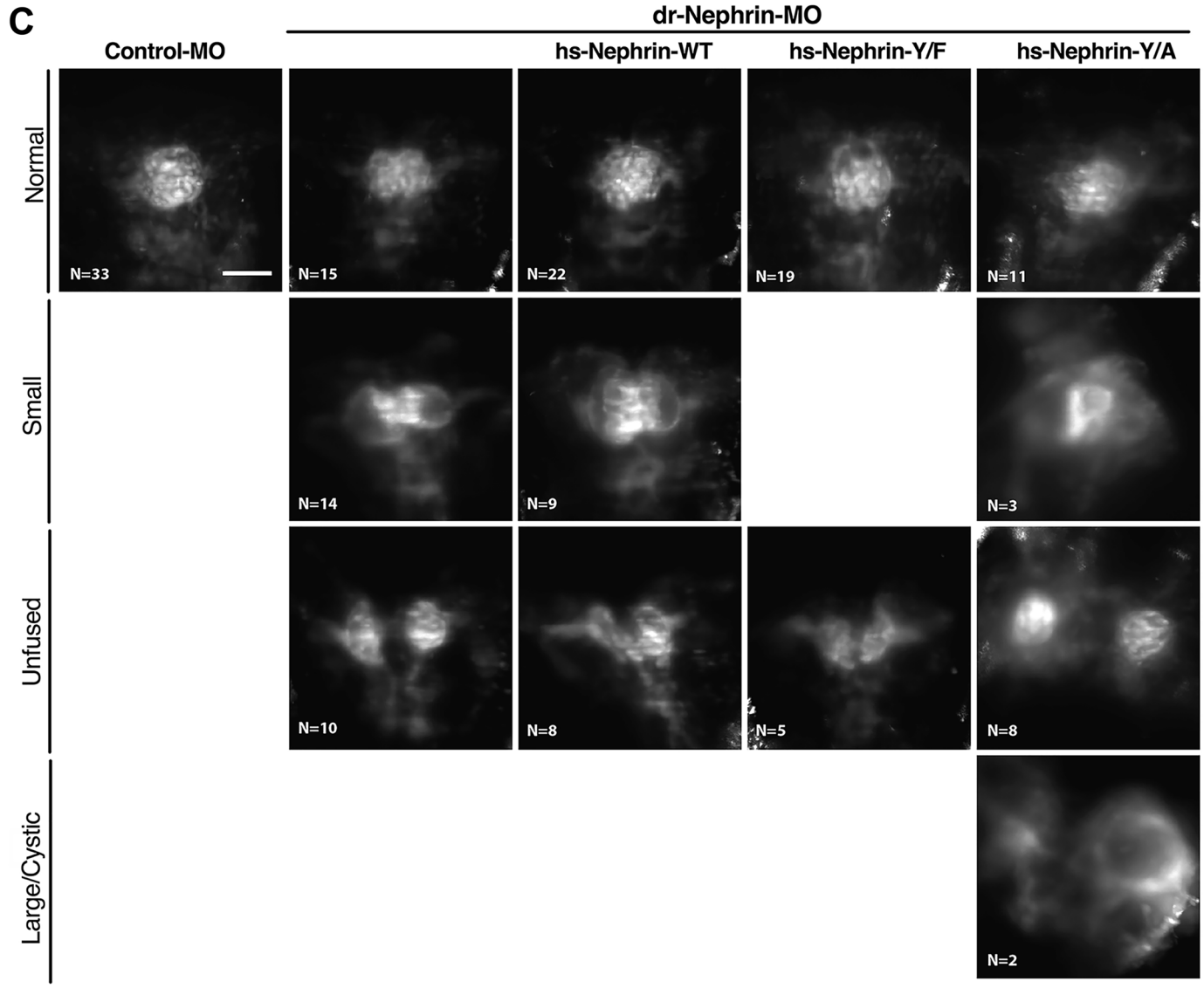

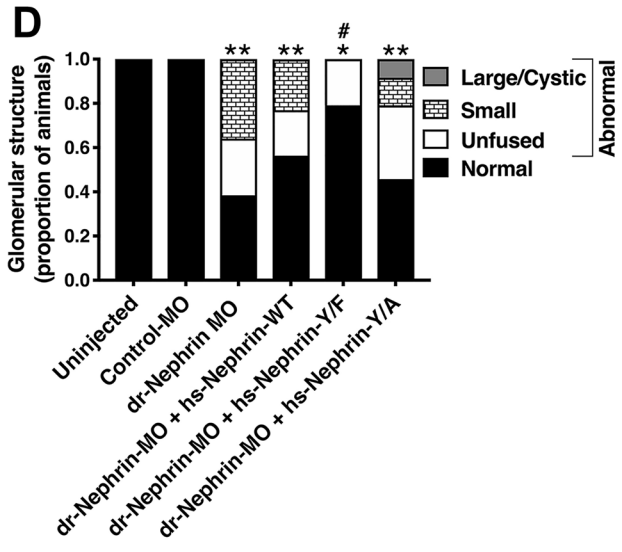

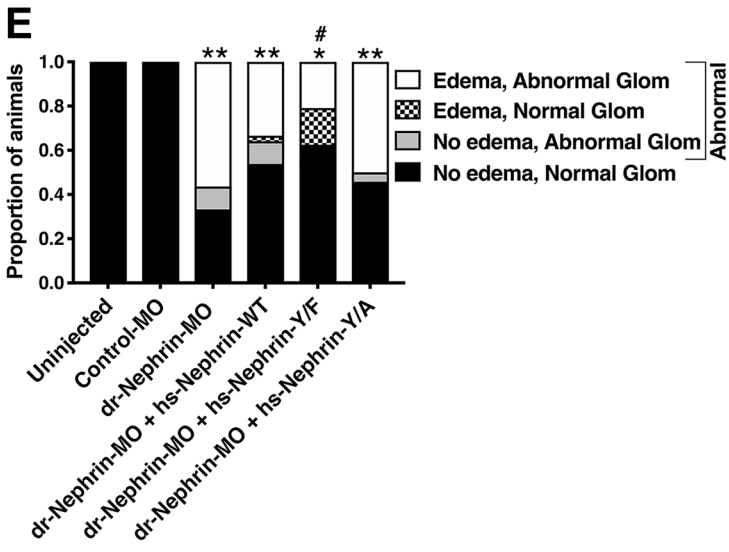

Figure 6 —*continued*

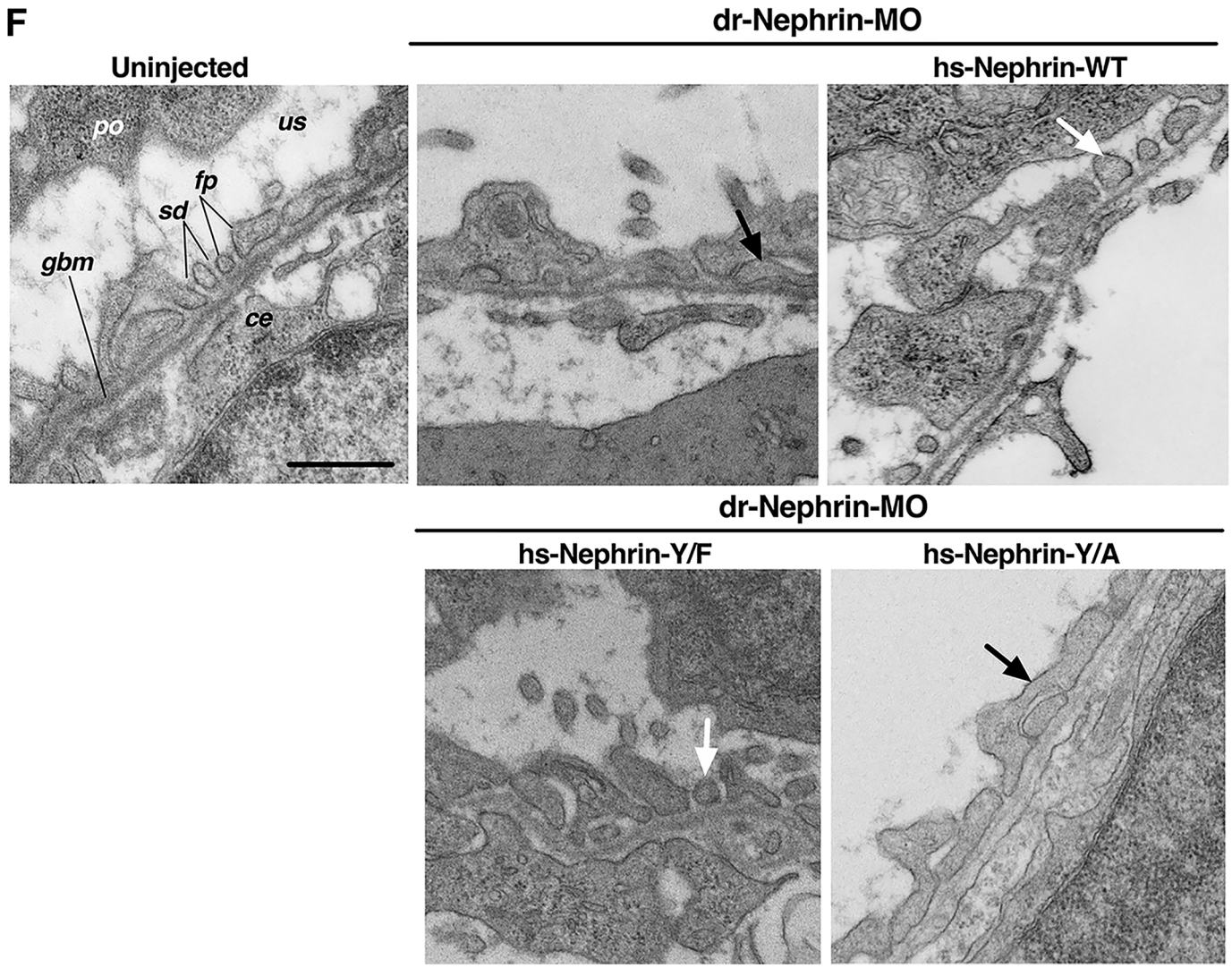

Figure 6 —*continued*

embryos (Fig. 6). Conversely, hs-Nephrin-Y^{1139}A failed to rescue, having phenotypes similar to nephrin depletion. Moreover, hs-Nephrin-Y^{1139}A alone exhibited abnormal glomerular structures, similar to those observed in nephrin morphants co-injected with hs-Nephrin-Y^{1139}A, suggesting that the Y^{1139}A mutation has dominant-negative effects during glomerular development (Fig. 7*B versus* Fig. 6*D*). Taken together, our data strongly support the view proposed by Grahammer *et al.* (9) that the slit diaphragm represents a highly dynamic, cell–cell contact forming an adjustable barrier within the renal filtration apparatus.

Podocyte differentiation requires recruitment of the slit diaphragm–specific, neuronal junction proteins to specialized membrane domains, and endocytic trafficking contributes to this process (9, 13, 14). We propose that the Y^{1139}RSL motif helps to form a slit diaphragm by recruiting nephrin to the correct location at the plasma membrane of developing podocytes. It has been shown that clathrin-dependent endocytosis mediated by the YRSL motif in the neuronal L1CAM creates spatial asymmetry in adhesive interactions with the environment and is critical for the physiologic sorting of axonal growth cone, whereas mutations of the *L1CAM* gene cause severe developmental anomalies in the human nervous system (38–42). Thus, the YRSL motif in diverse proteins may facilitate differentiation of podocytes and neurons by similar mechanisms. Our data strengthen the evidence for shared biological characteristics of podocytes and neurons (43, 44).

Different endocytic motifs help to diversify nephrin subcellular localization and function. For example, nephrin phosphorylation at residues Tyr^{1176} and Tyr^{1193} triggers its internalization via lipid raft–mediated endocytosis (45). By contrast, phosphorylation of the residue Tyr^{1193} inhibits β-arrestin–mediated, clathrin-dependent nephrin endocytosis, resulting in increased nephrin signaling (46). The Tyr^{1193} residue exists in the context of another Y*XX*Ø-type motif, Y^{1193}DEV, suggesting that the phosphorylation of Tyr^{1193} may also inhibit clathrin-dependent nephrin endocytosis mediated by Y^{1193}DEV (15, 47). As discussed above, the decrease rather than complete blockade of Nephrin-Y^{1139}A entry into CCVs is consistent with the presence of additional endocytic motifs directing clathrin-dependent endocytosis of human nephrin (Fig. 2). The YDEV sequence is present in the rat nephrin and may be responsible

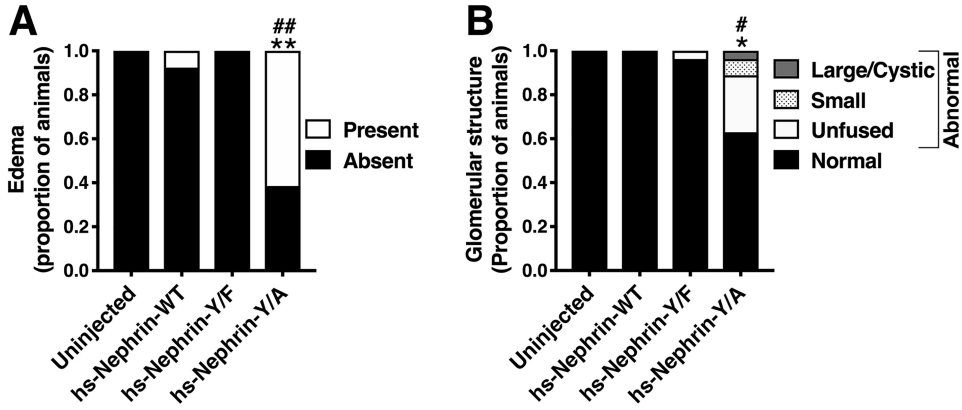

Figure 7. The hs-Nephrin-Y^{1139}A mutant has dominant-negative effects on the dr-Nephrin function in zebrafish embryos. *A*, animals untreated or injected with hs-Nephrin-WT, hs-Nephrin-Y^{1139}F, or hs-Nephrin-Y^{1139}A were imaged in bright field at 4 dpf. Additionally, shown are proportions of animals with abnormal glomerular organization patterns. $n = 15–40$ animals/condition. *B*, proportion of Tg(wt1a:GFP) animals with normal or abnormal glomerular patterns per denoted treatment were compared examined by a SPIM microscope. $n = 17–33$ animals/condition. Additionally, shown are the proportion of animals with specific patterns as subgroups in the abnormal glomerular organization group. *, $p < 0.05$; **, $p < 0.0001$ *versus* hs-Nephrin-WT. #, $p < 0.05$; ##, $p < 0.0001$ *versus* hs-Nephrin-Y/F.

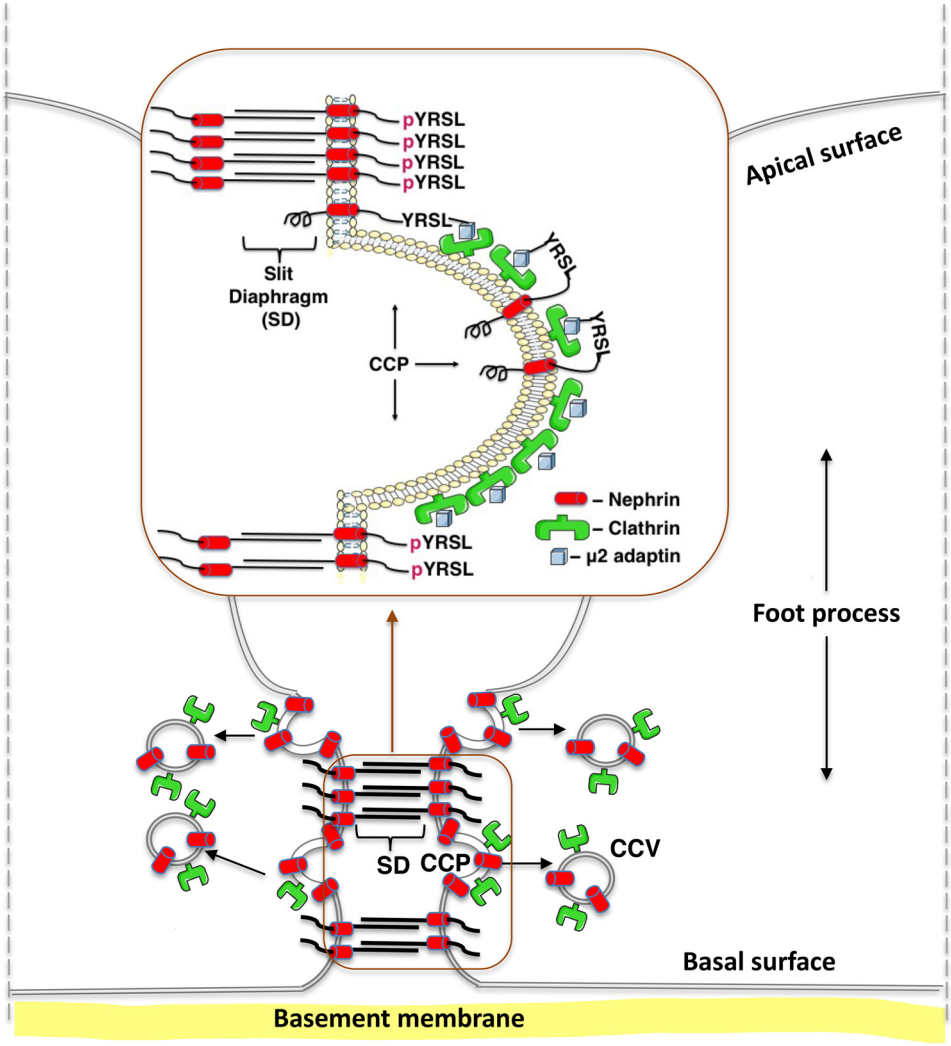

Figure 8. Model of the proposed role of the nephrin Y^{1139}RSL motif during podocyte development. Upon dephosphorylation of the amino acid residue Tyr^{1139} (YRSL), nephrin interacts with the μ2 adaptin of AP-2, followed by recruitment to CCPs, endocytosis in CCVs, and post-endocytic trafficking in recycling endosomes. We propose that the Y^{1139}RSL-mediated endocytosis and post-endocytic trafficking maintain the dynamic nephrin turnover and facilitate nephrin delivery to specialized membrane domains between neighboring foot processes, leading to organization into the functional slit diaphragm. The slit diaphragm dynamics are regulated by the state of nephrin phosphorylation at residue Tyr^{1139} (pYRSL). Upon phosphorylation, nephrin can be retained at the plasma membrane, leading to formation of homophilic interactions with nephrin from a neighboring foot process.

for its endocytosis via a clathrin-dependent pathway (Fig. S4). Nephrin multisequence alignment by MUSCLE (multisequence alignment with high accuracy and high throughput) demonstrated that YRSL is expressed only in primates (Fig. S1) (48). Expression of different endocytic motifs in homologous proteins has been reported previously. For example, SoRCS1, a member of the Vps10p domain receptor family and susceptibility gene for diabetes mellitus type 2, is internalized via a tyrosine-based endocytic motif in mice and via the D*XX*LL-type motif in humans (49). The reason why species evolve to utilize alternative endocytic motifs is not entirely clear but may be influenced by specific habitats. Nephrin expressed in the insulin-producing pancreatic β-cells also contains the Y^{1139}RSL motif (50–53). This is in contrast to the tissue-specific expression of the YRSL motif in L1CAM (54, 55).

Studies have shown that podocyte injury may result from defects in lipid raft– or clathrin–mediated nephrin endocytosis, and nephrin mislocalization has been observed in different forms of kidney disease (56–61). For example, phosphorylation of the residues Thr^{1120} and Thr^{1125} facilitates nephrin interaction with β-arrestin and induces nephrin endocytosis during hyperglycemia (62–64), whereas phosphorylation of the Tyr^{1193} and Tyr^{1217} residues facilitates nephrin endocytosis in a ShcA-dependent manner during PAN nephrosis (65). Our *in vivo* data demonstrate that disorder of the Y^{1139}RSL-mediated clathrin-dependent nephrin endocytosis impairs the slit diaphragm formation.

Zebrafish has been validated as an important model for studies of human podocytopathies, and the advantages include high fecundity and rapid development of pronephros containing the structural components of the slit diaphragm (66). Glomeruli of zebrafish pronephros fuse by 2 dpf and become functional by 3 dpf, but podocytes are not fully mature until 4 dpf (34–37). Thus, we used glomerular fusion as a descriptor for the maturation of pronephros by imaging at 4 dpf. Fukuyo *et al.* (32) showed that glomerular development is markedly disrupted in nephrin morphants. Our studies provide additional characterization and range of defects in glomerular development, including previously unreported failure of glomerular fusion (Fig. 6*C*). It is conceivable that nephrin plays a role in the fusion of nephron primordia because expression of nephrin mRNA is detected already at 34 hpf in the pair of epithelial vesicles forming the nephron primordia that fuse at the midline by 2 dpf (36). Rescue of the unfused phenotype in nephrin morphants by hs-Nephrin-WT or hs-Nephrin-Y^{1139}F and not hs-Nephrin-Y^{1139}A strongly supports the role of endocytic nephrin turnover in the glomerular fusion. Studies have shown that pronephric failure in zebrafish embryos causes generalized edema due to altered osmoregulation observed after 3 dpf, and Fukuyo *et al.* showed that human nephrin can rescue phenotypes associated with nephrin morphants, including edema (32, 34). Partial rescue of the edematous phenotype in zebrafish morphants co-injected with hs-Nephrin-WT or hs-Nephrin-Y^{1139}F and not hs-Nephrin-Y^{1139}A strongly supports the role of endocytic nephrin turnover in pronephric development (Fig. 6, *C* and *D*).

The WES and WGS analysis of nephrin Y^{1139}RSL motif demonstrates lack of genetic variation at nucleotide positions affecting residue Tyr^{1139} or Leu^{1142}. The allele frequencies of variants affecting Arg^{1140} and Ser^{1141}, including the pathogenic allele resulting in R^{1140}C, are rare in the population. This low-level presence can be consistent with alleles that transmit their pathogenicity in an autosomal recessive manner. The complete absence of missense variation affecting Tyr^{1139} and Leu^{1142} could imply strong negative selection acting at this position and further strengthens our conclusion regarding their particular importance.

Experimental procedures

Antibodies and reagents

The following anti-nephrin antibodies were used: 50A9 (mouse monoclonal raised against the extracellular domain of nephrin; gift from Dr. Karl Tryggvason, Karolinska Institute, Stockholm, Sweden), N-20 (rabbit polyclonal; Santa Cruz Biotechnology, Inc.), and pAB2 (rabbit polyclonal), as described previously (67). Other antibodies used were anti-GFP (mouse monoclonal JL8; Clontech), anti-clathrin heavy chain (mouse monoclonal; BD Biosciences), anti-μ2 adaptin (mouse monoclonal AP50 (BD Biosciences) or chicken polyclonal AP2M1 (ProSci Inc., Powy, CA)), anti-podocin (rabbit monoclonal, Sigma-Aldrich), rabbit polyclonal anti-Wilms tumor protein 1 (WT1), anti-caveolin-1 (rabbit polyclonal, Cell Signaling Technology, Danvers, MA), mouse monoclonal anti-CD2AP and goat polyclonal anti-dynamin II (Santa Cruz Biotechnology), anti-phosphotyrosine antibody 4G10 horseradish peroxidase conjugate (mouse monoclonal, Millipore, Temecula, CA), anti-ezrin (mouse monoclonal; BD Transduction Laboratories), and anti-actin (mouse monoclonal AC-15 or rabbit polyclonal; Sigma-Aldrich). Horseradish peroxidase–conjugated goat anti-mouse and goat anti-rabbit secondary antibodies (Bio-Rad), Alexa Fluor 555–conjugated goat anti-mouse IgG, and Alexa Fluor 488 – conjugated goat anti-rabbit IgG (Thermo Scientific) were used. All antibodies were used at the concentrations recommended by the manufacturer or as indicated in the figure legends.

Cells and cell culture

The T-SV40 immortalized human podocytes were a gift from Dr. J. D. Sraer (INSERM, Paris, France) (68). Podocytes were maintained in optimized RPMI 1640 medium (Cellgro, Manassas, VA) supplemented with 10% fetal bovine serum (Gibco), 50 units/ml penicillin and 50 mg/ml streptomycin, 2 mM L-glutamine (Sigma-Aldrich), and 5 ng/ml insulin-transferrin-selenium (Cellgro), as described previously (68, 69). These cells endogenously express several podocyte-specific proteins, including podocin, CD2AP, and WT1 (Fig. S1). However, endogenous nephrin expression was not detected, and podocytes were transfected with human nephrin plasmids. Following transient transfection with plasmid DNA or stable transduction with lentiviral particles, podocytes were seeded on plastic tissue culture plates or dishes (Corning Corp.) coated with 10% purified collagen (PureCol™, Advanced Biomatrix, San Diego, CA) or glass coverslips and cultured as described for individual experiments.

Plasmids and transient transfection

cDNA encoding full-length human nephrin (NM_004646.1) was amplified from the human cDNA library using the 5′ and 3′ rapid amplification of cDNA ends (Marathon™ cDNA amplification kit, (Clontech) and subcloned by PCR into the pCDNA 3.1 vector (Nephrin-WT). To construct Nephrin-$Y^{1139}F$ and Nephrin-$Y^{1139}A$, the cDNA encoding Nephrin-WT was mutated using the QuikChange™ II XL site-directed mutagenesis kit (Stratagene, La Jolla, CA). Constructs were sequence-verified by ABI PRISM dye terminator cycle sequencing (Applied Biosystems, Foster City, CA). We expressed untagged nephrin because the addition of a tag may alter protein trafficking. Transfection of cells with plasmids was performed using FuGENE6 (Roche Applied Science), according to the manufacturer's instructions. Rat dynamin 2 K44A (DynK44A) plasmid in pEGFP-N1 vector was received from Dr. William Guggino (Johns Hopkins University, Baltimore, MD) (70).

Stable transduction

To establish a podocyte cell line stably expressing human Nephrin-WT, the T-SV40 immortalized human podocytes were stably transduced with lentiviral particles containing the human Nephrin-WT plasmid (Precision LentiORF accession BC156195 clone ID: PLOHS_100061574) in pLOC lentiviral vector (Thermo Scientific). Lentiviral particles containing Nephrin-$Y^{1139}F$ or Nephrin-$Y^{1139}A$ in pLOC vector were produced at the University of Pittsburgh Viral Core Facility. Selection of podocytes stably expressing nephrin plasmids was carried out with blasticidin S, and culture of stably transduced podocytes was carried out as described above.

Biochemical determination of the plasma membrane nephrin

Podocytes grown to confluence on collagen-coated tissue culture plates were rapidly cooled to 4 °C to stop protein trafficking. Plasma membrane proteins were labeled with the plasma membrane–impermeable EZ-Link™ Sulfo-NHS-LC-Biotin (Pierce) followed by cell lysis in buffer containing 25 mM HEPES, pH 8.0, 1% Triton, 10% glycerol, and Complete Protease Inhibitor Mixture (Roche Applied Science). Biotinylated proteins were isolated from the whole-cell lysate (WCL) by incubation with streptavidin-agarose beads as described previously (24). All steps were performed at 4 °C. As previously demonstrated with appropriate intracellular controls, only proteins present at the cell surface were accessible to biotin (26). Immunoblotting for an intracellular protein, such as ezrin, was used as a control to confirm the absence of intracellular proteins in the biotinylated protein samples. Incubation of podocytes with cycloheximide (Sigma-Aldrich; 20 μg/ml), a protein synthesis inhibitor, was performed at 37 °C, and the disappearance of Nephrin-WT, Nephrin-$Y^{1139}F$, and Nephrin-$Y^{1139}A$ from the plasma membrane was monitored over time, as described previously (24). The half-lives were calculated using the one-phase exponential decay model, with plateau and span parameters constrained to 0 and 100, respectively (71). Biotinylated nephrin was visualized by immunoblotting with antibody 50A9 and an anti-mouse horseradish peroxidase antibody using the Western Lightning™ Plus-ECL detection system (Perkin-Elmer Life Sciences) followed by chemiluminescence. Quantification of biotinylated proteins was performed by ImageJ (National Institutes of Health, Bethesda, ND) densitometry using exposures within the linear dynamic range of the film.

Density gradient separation and differential centrifugation of CCVs

Confluent podocytes expressing Nephrin-WT, Nephrin-$Y^{1139}F$, or Nephrin-$Y^{1139}A$ were first rapidly cooled to 4 °C to stop endocytic trafficking and synchronize the cell surface protein abundance, and subsequently cells were rapidly warmed to 37 °C for 7.5 min to induce endocytic uptake of proteins into CCVs, followed by rapid cooling to 4 °C and CCV isolation at 4 °C as described in our previous publication (24). To isolate CCVs, subcellular fractionation was performed by density gradient and differential centrifugation as described previously (24). After washing with ice-cold PBS supplemented with Complete Protease Inhibitor Mixture and PhosSTOP (Roche Applied Science) at 4 °C, podocytes were harvested in Buffer A (BA), pH 6.5, containing 1 M MES, 10 mM EGTA, and 0.5 M $MgCl_2$, and homogenized in a glass-Teflon homogenizer using 20 strokes at 1500 rpm. To prepare the microsomal fraction (P2) containing CCVs, the homogenates were centrifuged at 17,000 × *g* for 20 min in a Sorvall Biofuge at 4 °C, and the resultant supernatant (S1) was centrifuged at 56,000 × *g* for 60 min at 4 °C in a Sorvall swinging bucket rotor TH641 in a Sorvall WX 80 Ultra ultracentrifuge. The resultant pellet (P2) was resuspended in BA and homogenized with five strokes at 1500 rpm, fresh BA was added, and the suspension was passed through a syringe barrel equipped with a 27-gauge ⅝-inch needle. To pellet CCVs through the sucrose cushion, the P2 suspension was collected in 12.2-ml polyallomer tubes (Sorvall, 14-mm diameter), and the D_2O-sucrose solution (8% (w/v) final) was injected at the bottom of the tube underneath the P2 suspension and centrifuged at 120,000 × *g* for 2 h at 4 °C in a Sorvall swinging bucket rotor TH641 in a Sorvall WX 80 Ultra ultracentrifuge. After discarding the supernatant, the pelleted CCVs were resuspended in a small volume of BA and collected.

Immunoprecipitation and immunoblotting

Podocytes transfected with the Nephrin-WT, Nephrin-$Y^{1139}F$, or Nephrin-$Y^{1139}A$ plasmids were cultured for 48–72 h to form monolayers and were incubated for 15 min at 37 °C with buffer containing 50 mM HEPES, pH 7.4, 40 μM pervanadate, 1 mM $MgCl_2$, and 0.1 mM $CaCl_2$. Pervanadate was prepared from sodium orthovanadate (Sigma-Aldrich) in 20 mM HEPES as described previously (72). Cells were lysed in an immunoprecipitation (IP) buffer containing 150 mM NaCl, 50 mM HEPES, pH 7.4, 1% IGEPAL CA-630 (Sigma-Aldrich), 5 mM $MgCl_2$, 5 mM EDTA, 1 mM EGTA, 30 mM NaF, 1 mM Na_3VO_4, Complete Protease Inhibitor Mixture, and PhosSTOP as described previously (24). After centrifugation at 14,000 × *g* for 15 min to pellet insoluble material, the soluble lysates were precleared by incubation with protein G–Sepharose beads conjugated with the nonimmune mouse IgG (DAKO North America, Inc., Carpinteria, CA) (Pierce) at 4 °C. The precleared lysates were added to the protein G–Sepharose bead–antibody complexes. Nephrin was immunoprecipitated by incubation

with the mouse antibody 50A9. After washing the protein G–Sepharose bead–antibody complexes with the IP buffer, immunoprecipitated proteins were eluted by incubation at 85 °C for 5 min in sample buffer (Bio-Rad) containing 100 mM DTT. Immunoprecipitated proteins were separated by SDS-PAGE using 7.5% gels (Bio-Rad) and analyzed by immunoblotting. The immunoreactive bands were visualized with the Western Lightning™ Plus-ECL detection system.

Cell migration assay

Podocyte migration was studied by a method established previously (73). Podocytes stably expressing Nephrin-WT, Nephrin-Y^{1139}F, or Nephrin-Y^{1139}A were cultured to confluence on collagen I– coated 60-mm dishes. One scratch along the diameter of each dish was made using the P200 pipette tip, and reference points were made on the bottom of the dish. Cells were washed once with cell culture medium to remove cell debris along the scratch and incubated at 37 °C. Cells were allowed to migrate into the scratch at 37 °C for up to 24 h, at which time the podocytes expressing Nephrin-WT completely closed the wound. Cells were washed with PBS and fixed with 2% paraformaldehyde. Images at ×10 magnification were obtained with a wide field microscope, and the cell nuclei were counted using the ImageJ software. The number of migrated cells were counted in four fields per condition.

Zebrafish husbandry

Zebrafish were reared according to established protocols (74), which were approved by the University of Pittsburgh Institutional Animal Care and Use Committee.

Injections of zebrafish embryos and efficiency testing

The validated zebrafish nephrin MO for the splice blocking of nephrin-exon 25 (dr-Nephrin-MO, 5′-TGC ACC AAC ACG ACT CAC CTC TG-3′) and standard control oligonucleotide (Control-MO, 5′-CCT CTT ACC TCA GTT ACA ATT TAT A-3′) were synthesized by Gene Tools LLC (Philomath, OR), as described previously (32). Human Nephrin-WT, Nephrin-Y^{1139}F, or Nephrin-Y^{1139}A was cloned into pcDNA3.1; synthesis of capped RNA from these plasmids was generated utilizing the mMESSAGE mMACHINE™ T7 Transcription Kit (Invitrogen) (32). Tg(wt1a:gfp) zebrafish embryos were injected with 0.5 pg of synthetic human nephrin transcripts directly into the one-cell blastomere; in rescue experiments, this was subsequently followed by injection of 5.75 ng of dr-Nephrin-MO into the yolk. Embryos developed at 28 °C for 4 days in E3 embryo medium containing 30 μg/ml phenylthiourea to inhibit pigment deposition. Splice blocking was verified by RT-PCR (32). Total RNA was isolated from embryos at 4 dpf, and RT-PCR was done using GeneAmp Fast master mix (Applied Biosystems, Foster City, CA). The primer set used was as follows: 5′-GGC AGG ATC TGC AAG CTA CAT-3′ and 5′-CTC AGG GCC TTC AGG GTG AG-3′ (32). The primers span the regions of nephrin DNA corresponding to exon junctions 24–25, 25–26, and 26–27 so as to identify mis-splicing in these exon regions caused by dr-Nephrin-MO. To compare PCR products between Random-MO and dr-Nephrin-MO, 5 μl of each PCR product was run on 2% agarose gel, followed by gel extraction using the QIAquick Gel Extraction Kit (Qiagen, Hilden, Germany). After elution of PCR products from columns, the concentration and purity were measured on the Nanodrop (Thermo Scientific) and sequenced using the same primers as those to amplify the PCR products. Sequencing of purified gel-extracted PCR products was only successful on the full-size band in the Control-MO–treated embryos and verified the amplicon expected from the full-size product. Sequencing of the smallest band in the dr-Nephrin-MO PCR products revealed deletion of 47 bp corresponding to exon 25, resulting in a frameshift and nonsense translation of the subsequent exons, responsible for translation of the intracellular nephrin domain.

SPIM of zebrafish embryos

Animals were anesthetized in 160 μg/ml tricaine and 200 μM Tris, pH 9.0, in E3 medium. Whole animals were imaged in bright field using Qcapture version 3.1.2 software under a Leica MZ16 stereomicroscope mounted with a Retiga 1300 CCD camera (QImaging). Fluorescent images of the zebrafish glomeruli were captured using μManager (Open Imaging, Inc.) under a SPIM microscope assembled as shown on the OpenSPIM Wiki with dual plane illumination to provide nearly uniform illumination along the plane. All images were projected and processed in Fiji (75).

TEM of the zebrafish glomerular region

Animals were fixed at 4 dpf in cold 2.5% glutaraldehyde in 0.01 M PBS. The specimens were rinsed in PBS, post-fixed in 1% osmium tetroxide with 1% potassium ferricyanide, rinsed in PBS, dehydrated through a graded series of ethanol and propylene oxide, and embedded in Poly/Bed® 812 (Luft formulations) and processed using standard protocols for TEM as outlined by the Center of Biologic Imaging (University of Pittsburgh). Ultrathin sections (65 nm) were stained with uranyl acetate and Reynold's lead citrate and examined on JEOL 1011 TEM with a side mount AMT 2k digital camera (Advanced Microscopy Techniques, Danvers, MA). Images were then processed in Fiji.

Data analysis and statistics

Statistical analysis of the data was performed using GraphPad Prism version 4.0 for Macintosh (GraphPad Software Inc., San Diego, CA). The half-lives were calculated using the one-phase exponential decay model, with plateau and span parameters constrained to 0 and 100, respectively (71). The half-life means were compared by two-tailed t test with assumed unequal variance. The means for the remaining data were compared by a two-tailed t test. $p < 0.05$ was considered significant. Data are expressed as mean ± S.E.

In the zebrafish studies, for analyzing both body appearance and glomerular architecture, a two-sided Fisher exact test was used to statistically compare groups. For glomerular architecture, all animals that had abnormal glomerular structures were summed together in the use of this contingency test. $p < 0.05$ was considered significant, and $p < 0.0001$ was considered very significant.

Author contributions—E. B. E. and H. J. acquired and analyzed data and drafted sections of the manuscript; M. S., D. B. S, and K. Y. acquired and analyzed data; S. M.-M., M. G. S., N. A. H., and A. S.-U. contributed to the conception and design of the study; all authors approved the final version.

Acknowledgments—We thank Drs. J. D. Sraer, C. Tryggvason, and W. Guggino for reagents. We thank Kristine M. Cihil, Jacob E. Winschel, and Corey Toocheck for technical assistance.

References

1. Kamiguchi, H., Hlavin, M. L., and Lemmon, V. (1998) Role of L1 in neural development: what the knockouts tell us. *Mol. Cell Neurosci.* **12,** 48–55 CrossRef Medline
2. Brümmendorf, T., and Lemmon, V. (2001) Immunoglobulin superfamily receptors: cis-interactions, intracellular adapters and alternative splicing regulate adhesion. *Curr. Opin. Cell Biol.* **13,** 611–618 CrossRef Medline
3. Kestilä, M., Lenkkeri, U., Männikkö, M., Lamerdin, J., McCready, P., Putaala, H., Ruotsalainen, V., Morita, T., Nissinen, M., Herva, R., Kashtan, C. E., Peltonen, L., Holmberg, C., Olsen, A., and Tryggvason, K. (1998) Positionally cloned gene for a novel glomerular protein–nephrin–is mutated in congenital nephrotic syndrome. *Mol. Cell* **1,** 575–582 CrossRef Medline
4. Lenkkeri, U., Mannikkö, M., McCready, P., Lamerdin, J., Gribouval, O., Niaudet, P. M., Antignac, C. K., Kashtan, C. E., Homberg, C., Olsen, A., Kestilä, M., and Tryggvason, K. (1999) Structure of the gene for congenital nephrotic syndrome of the finnish type (NPHS1) and characterization of mutations. *Am. J. Hum. Genet.* **64,** 51–61 CrossRef Medline
5. Patrakka, J., Kestilä, M., Wartiovaara, J., Ruotsalainen, V., Tissari, P., Lenkkeri, U., Männikkö, M., Visapää, I., Holmberg, C., Rapola, J., Tryggvason, K., and Jalanko, H. (2000) Congenital nephrotic syndrome (NPHS1): features resulting from different mutations in Finnish patients. *Kidney Int.* **58,** 972–980 CrossRef Medline
6. Asanuma, K., and Mundel, P. (2003) The role of podocytes in glomerular pathobiology. *Clin. Exp. Nephrol.* **7,** 255–259 CrossRef Medline
7. Haraldsson, B., and Jeansson, M. (2009) Glomerular filtration barrier. *Curr. Opin. Nephrol. Hypertens.* **18,** 331–335 CrossRef Medline
8. Hinkes, B. G., Mucha, B., Vlangos, C. N., Gbadegesin, R., Liu, J., Hasselbacher, K., Hangan, D., Ozaltin, F., Zenker, M., Hildebrandt, F., and Arbeitsgemeinschaft für Paediatrische Nephrologie Study Group (2007) Nephrotic syndrome in the first year of life: two thirds of cases are caused by mutations in 4 genes (NPHS1, NPHS2, WT1, and LAMB2). *Pediatrics* **119,** e907–e919 CrossRef Medline
9. Grahammer, F., Wigge, C., Schell, C., Kretz, O., Patrakka, J., Schneider, S., Klose, M., Kind, J., Arnold, S. J., Habermann, A., Bräuniger, R., Rinschen, M. M., Völker, L., Bregenzer, A., Rubbenstroth, D., Boerries, M., *et al.* (2016) A flexible, multilayered protein scaffold maintains the slit in between glomerular podocytes. *JCI Insight* **1,** 86177 CrossRef Medline
10. Conti, S., Perico, L., Grahammer, F., and Huber, T. B. (2017) The long journey through renal filtration: new pieces in the puzzle of slit diaphragm architecture. *Curr. Opin. Nephrol. Hypertens.* **26,** 148–153 CrossRef Medline
11. Huber, T. B., and Benzing, T. (2005) The slit diaphragm: a signaling platform to regulate podocyte function. *Curr. Opin. Nephrol. Hypertens.* **14,** 211–216 CrossRef Medline
12. Welsh, G. I., and Saleem, M. A. (2010) Nephrin-signature molecule of the glomerular podocyte? *J. Pathol.* **220,** 328–337 CrossRef Medline
13. Babayeva, S., Rocque, B., Aoudjit, L., Zilber, Y., Li, J., Baldwin, C., Kawachi, H., Takano, T., and Torban, E. (2013) Planar cell polarity pathway regulates nephrin endocytosis in developing podocytes. *J. Biol. Chem.* **288,** 24035–24048 CrossRef Medline
14. Swiatecka-Urban, A. (2013) Membrane trafficking in podocyte health and disease. *Pediatr. Nephrol.* **28,** 1723–1737 CrossRef Medline
15. Pandey, K. N. (2009) Functional roles of short sequence motifs in the endocytosis of membrane receptors. *Front. Biosci.* **14,** 5339–5360 Medline CrossRef
16. Schoeb, D. S., Chernin, G., Heeringa, S. F., Matejas, V., Held, S., Vega-Warner, V., Bockenhauer, D., Vlangos, C. N., Moorani, K. N., Neuhaus, T. J., Kari, J. A., MacDonald, J., Saisawat, P., Ashraf, S., Ovunc, B., *et al.* (2010) Nineteen novel NPHS1 mutations in a worldwide cohort of patients with congenital nephrotic syndrome (CNS). *Nephrol. Dial. Transplant.* **25,** 2970–2976 CrossRef Medline
17. Mousavi, S. A., Malerød, L., Berg, T., and Kjeken, R. (2004) Clathrin-dependent endocytosis. *Biochem. J.* **377,** 1–16 CrossRef Medline
18. Hinshaw, J. E., and Schmid, S. L. (1995) Dynamin self-assembles into rings suggesting a mechanism for coated vesicle budding. *Nature* **374,** 190–192 CrossRef Medline
19. Takei, K., McPherson, P. S., Schmid, S. L., and De Camilli, P. (1995) Tubular membrane invaginations coated by dynamin rings are induced by GTP-γS in nerve terminals. *Nature* **374,** 186–190 CrossRef Medline
20. Nishimura, N., and Sasaki, T. (2009) Rab family small G proteins in regulation of epithelial apical junctions. *Front. Biosci.* (*Landmark Ed.*) **14,** 2115–2129 Medline
21. Mercer, J., Schelhaas, M., and Helenius, A. (2010) Virus entry by endocytosis. *Annu. Rev. Biochem.* **79,** 803–833 CrossRef Medline
22. Ohno, H., Stewart, J., Fournier, M. C., Bosshart, H., Rhee, I., Miyatake, S., Saito, T., Gallusser, A., Kirchhausen, T., and Bonifacino, J. S. (1995) Interaction of tyrosine-based sorting signals with clathrin-associated proteins. *Science* **269,** 1872–1875 CrossRef Medline
23. Bonifacino, J. S., and Traub, L. M. (2003) Signals for sorting of transmembrane proteins to endosomes and lysosomes. *Annu. Rev. Biochem.* **72,** 395–447 CrossRef Medline
24. Cihil, K. M., Ellinger, P., Fellows, A., Stolz, D. B., Madden, D. R., and Swiatecka-Urban, A. (2012) Disabled-2 protein facilitates assembly polypeptide-2-independent recruitment of cystic fibrosis transmembrane conductance regulator to endocytic vesicles in polarized human airway epithelial cells. *J. Biol. Chem.* **287,** 15087–15099 CrossRef Medline
25. Marks, M. S., Woodruff, L., Ohno, H., and Bonifacino, J. S. (1996) Protein targeting by tyrosine- and di-leucine-based signals: evidence for distinct saturable components. *J. Cell Biol.* **135,** 341–354 CrossRef Medline
26. Ye, S., Cihil, K., Stolz, D. B., Pilewski, J. M., Stanton, B. A., and Swiatecka-Urban, A. (2010) c-Cbl facilitates endocytosis and lysosomal degradation of cystic fibrosis transmembrane conductance regulator in human airway epithelial cells. *J. Biol. Chem.* **285,** 27008–27018 CrossRef Medline
27. Welsh, G. I., and Saleem, M. A. (2011) The podocyte cytoskeleton–key to a functioning glomerulus in health and disease. *Nat. Rev. Nephrol.* **8,** 14–21 CrossRef Medline
28. Reiser, J., Oh, J., Shirato, I., Asanuma, K., Hug, A., Mundel, T. M., Honey, K., Ishidoh, K., Kominami, E., Kreidberg, J. A., Tomino, Y., and Mundel, P. (2004) Podocyte migration during nephrotic syndrome requires a coordinated interplay between cathepsin L and α3 integrin. *J. Biol. Chem.* **279,** 34827–34832 CrossRef Medline
29. Datta, N., Lindfors, S., Miura, N., Saleem, M. A., and Lehtonen, S. (2016) Overexpression of transcription factor FOXC2 in cultured human podocytes upregulates injury markers and increases motility. *Exp. Cell Res.* **340,** 32–42 CrossRef Medline
30. Shankland, S. J. (2006) The podocyte's response to injury: role in proteinuria and glomerulosclerosis. *Kidney Int.* **69,** 2131–2147 CrossRef Medline
31. Lewko, B., and Stepinski, J. (2009) Hyperglycemia and mechanical stress: targeting the renal podocyte. *J. Cell. Physiol.* **221,** 288–295 CrossRef Medline
32. Fukuyo, Y., Nakamura, T., Bubenshchikova, E., Powell, R., Tsuji, T., Janknecht, R., and Obara, T. (2014) Nephrin and Podocin functions are highly conserved between the zebrafish pronephros and mammalian metanephros. *Mol. Med. Rep.* **9,** 457–465 CrossRef Medline
33. Bollig, F., Perner, B., Besenbeck, B., Köthe, S., Ebert, C., Taudien, S., and Englert, C. (2009) A highly conserved retinoic acid responsive element controls wt1a expression in the zebrafish pronephros. *Development* **136,** 2883–2892 CrossRef Medline
34. Drummond, I. A., Majumdar, A., Hentschel, H., Elger, M., Solnica-Krezel, L., Schier, A. F., Neuhauss, S. C., Stemple, D. L., Zwartkruis, F., Rangini, Z., Driever, W., and Fishman, M. C. (1998) Early development of the zebrafish pronephros and analysis of mutations affecting pronephric function. *Development* **125,** 4655–4667 Medline

35. Ichimura, K., Bubenshchikova, E., Powell, R., Fukuyo, Y., Nakamura, T., Tran, U., Oda, S., Tanaka, M., Wessely, O., Kurihara, H., Sakai, T., and Obara, T. (2012) A comparative analysis of glomerulus development in the pronephros of medaka and zebrafish. *PLoS One* **7,** e45286 CrossRef Medline
36. Ichimura, K., Fukuyo, Y., Nakamura, T., Powell, R., Sakai, T., Janknecht, R., and Obara, T. (2013) Developmental localization of nephrin in zebrafish and medaka pronephric glomerulus. *J. Histochem. Cytochem.* **61,** 313–324 CrossRef Medline
37. Kramer-Zucker, A. G., Wiessner, S., Jensen, A. M., and Drummond, I. A. (2005) Organization of the pronephric filtration apparatus in zebrafish requires Nephrin, Podocin and the FERM domain protein Mosaic eyes. *Dev. Biol.* **285,** 316–329 CrossRef Medline
38. Kamiguchi, H., Long, K. E., Pendergast, M., Schaefer, A. W., Rapoport, I., Kirchhausen, T., and Lemmon, V. (1998) The neural cell adhesion molecule L1 interacts with the AP-2 adaptor and is endocytosed via the clathrin-mediated pathway. *J. Neurosci.* **18,** 5311–5321 CrossRef Medline
39. Long, K. E., Asou, H., Snider, M. D., and Lemmon, V. (2001) The role of endocytosis in regulating L1-mediated adhesion. *J. Biol. Chem.* **276,** 1285–1290 CrossRef Medline
40. Schaefer, A. W., Kamei, Y., Kamiguchi, H., Wong, E. V., Rapoport, I., Kirchhausen, T., Beach, C. M., Landreth, G., Lemmon, S. K., and Lemmon, V. (2002) L1 endocytosis is controlled by a phosphorylation-dephosphorylation cycle stimulated by outside-in signaling by L1. *J. Cell Biol.* **157,** 1223–1232 CrossRef Medline
41. Gomez, T. M., and Letourneau, P. C. (2014) Actin dynamics in growth cone motility and navigation. *J. Neurochem.* **129,** 221–234 CrossRef Medline
42. Kamiguchi, H., and Yoshihara, F. (2001) The role of endocytic l1 trafficking in polarized adhesion and migration of nerve growth cones. *J. Neurosci.* **21,** 9194–9203 CrossRef Medline
43. Sun, Y., Zhang, H., Hu, R., Sun, J., Mao, X., Zhao, Z., Chen, Q., and Zhang, Z. (2014) The expression and significance of neuronal iconic proteins in podocytes. *PLoS One* **9,** e93999 CrossRef Medline
44. Sugie, A., Umetsu, D., Yasugi, T., Fischbach, K. F., and Tabata, T. (2010) Recognition of pre- and postsynaptic neurons via nephrin/NEPH1 homologs is a basis for the formation of the *Drosophila* retinotopic map. *Development* **137,** 3303–3313 CrossRef Medline
45. Qin, X. S., Tsukaguchi, H., Shono, A., Yamamoto, A., Kurihara, H., and Doi, T. (2009) Phosphorylation of nephrin triggers its internalization by raft-mediated endocytosis. *J. Am. Soc. Nephrol.* **20,** 2534–2545 CrossRef Medline
46. Quack, I., Rump, L. C., Gerke, P., Walther, I., Vinke, T., Vonend, O., Grunwald, T., and Sellin, L. (2006) β-Arrestin2 mediates nephrin endocytosis and impairs slit diaphragm integrity. *Proc. Natl. Acad. Sci. U.S.A.* **103,** 14110–14115 CrossRef Medline
47. Swiatecka-Urban, A. (2017) Endocytic trafficking at the mature podocyte slit diaphragm. *Front. Pediatr.* **5,** 32 CrossRef Medline
48. Edgar, R. C. (2004) MUSCLE: multiple sequence alignment with high accuracy and high throughput. *Nucleic Acids Res.* **32,** 1792–1797 CrossRef Medline
49. Nielsen, M. S., Keat, S. J., Hamati, J. W., Madsen, P., Gutzmann, J. J., Engelsberg, A., Pedersen, K. M., Gustafsen, C., Nykjaer, A., Gliemann, J., Hermans-Borgmeyer, I., Kuhl, D., Petersen, C. M., and Hermey, G. (2008) Different motifs regulate trafficking of SorCS1 isoforms. *Traffic* **9,** 980–994 CrossRef Medline
50. Palmén, T., Ahola, H., Palgi, J., Aaltonen, P., Luimula, P., Wang, S., Jaakkola, I., Knip, M., Otonkoski, T., and Holthöfer, H. (2001) Nephrin is expressed in the pancreatic beta cells. *Diabetologia* **44,** 1274–1280 CrossRef Medline
51. Fornoni, A., Jeon, J., Varona Santos, J., Cobianchi, L., Jauregui, A., Inverardi, L., Mandic, S. A., Bark, C., Johnson, K., McNamara, G., Pileggi, A., Molano, R. D., Reiser, J., Tryggvason, K., Kerjaschki, D., Berggren, P. O., Mundel, P., and Ricordi, C. (2010) Nephrin is expressed on the surface of insulin vesicles and facilitates glucose-stimulated insulin release. *Diabetes* **59,** 190–199 CrossRef Medline
52. Jeon, J., Leibiger, I., Moede, T., Walter, B., Faul, C., Maiguel, D., Villarreal, R., Guzman, J., Berggren, P. O., Mundel, P., Ricordi, C., Merscher-Gomez, S., and Fornoni, A. (2012) Dynamin-mediated Nephrin phosphorylation regulates glucose-stimulated insulin release in pancreatic beta cells. *J. Biol. Chem.* **287,** 28932–28942 CrossRef Medline
53. Kapodistria, K., Tsilibary, E. P., Politis, P., Moustardas, P., Charonis, A., and Kitsiou, P. (2015) Nephrin, a transmembrane protein, is involved in pancreatic beta-cell survival signaling. *Mol. Cell. Endocrinol.* **400,** 112–128 CrossRef Medline
54. Takeda, Y., Asou, H., Murakami, Y., Miura, M., Kobayashi, M., and Uyemura, K. (1996) A nonneuronal isoform of cell adhesion molecule L1: tissue-specific expression and functional analysis. *J. Neurochem.* **66,** 2338–2349 Medline
55. Reid, R. A., and Hemperly, J. J. (1992) Variants of human L1 cell adhesion molecule arise through alternate splicing of RNA. *J. Mol. Neurosci.* **3,** 127–135 CrossRef Medline
56. Langham, R. G., Kelly, D. J., Cox, A. J., Thomson, N. M., Holthöfer, H., Zaoui, P., Pinel, N., Cordonnier, D. J., and Gilbert, R. E. (2002) Proteinuria and the expression of the podocyte slit diaphragm protein, nephrin, in diabetic nephropathy: effects of angiotensin converting enzyme inhibition. *Diabetologia* **45,** 1572–1576 CrossRef Medline
57. Benigni, A., Gagliardini, E., Tomasoni, S., Abbate, M., Ruggenenti, P., Kalluri, R., and Remuzzi, G. (2004) Selective impairment of gene expression and assembly of nephrin in human diabetic nephropathy. *Kidney Int.* **65,** 2193–2200 CrossRef Medline
58. Shono, A., Tsukaguchi, H., Kitamura, A., Hiramoto, R., Qin, X. S., Doi, T., and Iijima, K. (2009) Predisposition to relapsing nephrotic syndrome by a nephrin mutation that interferes with assembly of functioning microdomains. *Hum. Mol. Genet.* **18,** 2943–2956 CrossRef Medline
59. Kim, J. J., Li, J. J., Jung, D. S., Kwak, S. J., Ryu, D. R., Yoo, T. H., Han, S. H., Choi, H. Y., Kim, H. J., Han, D. S., and Kang, S. W. (2007) Differential expression of nephrin according to glomerular size in early diabetic kidney disease. *J. Am. Soc. Nephrol.* **18,** 2303–2310 CrossRef Medline
60. Doublier, S., Ruotsalainen, V., Salvidio, G., Lupia, E., Biancone, L., Conaldi, P. G., Reponen, P., Tryggvason, K., and Camussi, G. (2001) Nephrin redistribution on podocytes is a potential mechanism for proteinuria in patients with primary acquired nephrotic syndrome. *Am. J. Pathol.* **158,** 1723–1731 CrossRef Medline
61. Doublier, S., Salvidio, G., Lupia, E., Ruotsalainen, V., Verzola, D., Deferrari, G., and Camussi, G. (2003) Nephrin expression is reduced in human diabetic nephropathy: evidence for a distinct role for glycated albumin and angiotensin II. *Diabetes* **52,** 1023–1030 CrossRef Medline
62. Tossidou, I., Teng, B., Menne, J., Shushakova, N., Park, J. K., Becker, J. U., Modde, F., Leitges, M., Haller, H., and Schiffer, M. (2010) Podocytic PKC-α is regulated in murine and human diabetes and mediates nephrin endocytosis. *PLoS One* **5,** e10185 CrossRef Medline
63. Menne, J., Meier, M., Park, J. K., Boehne, M., Kirsch, T., Lindschau, C., Ociepka, R., Leitges, M., Rinta-Valkama, J., Holthofer, H., and Haller, H. (2006) Nephrin loss in experimental diabetic nephropathy is prevented by deletion of protein kinase C α signaling *in-vivo*. *Kidney Int.* **70,** 1456–1462 CrossRef Medline
64. Quack, I., Woznowski, M., Potthoff, S. A., Palmer, R., Königshausen, E., Sivritas, S., Schiffer, M., Stegbauer, J., Vonend, O., Rump, L. C., and Sellin, L. (2011) PKC α mediates β-arrestin2-dependent nephrin endocytosis in hyperglycemia. *J. Biol. Chem.* **286,** 12959–12970 CrossRef Medline
65. Martin, C. E., Petersen, K. A., Aoudjit, L., Tilak, M., Eremina, V., Hardy, W. R., Quaggin, S. E., Takano, T., and Jones, N. (2018) ShcA adaptor protein promotes nephrin endocytosis and is upregulated in proteinuric nephropathies. *J. Am. Soc. Nephrol.* **29,** 92–103 CrossRef Medline
66. Schenk, H., Müller-Deile, J., Kinast, M., and Schiffer, M. (2017) Disease modeling in genetic kidney diseases: zebrafish. *Cell Tissue Res.* **369,** 127–141 CrossRef Medline
67. Ito, N., Nishibori, Y., Ito, Y., Takagi, H., Akimoto, Y., Kudo, A., Asanuma, K., Sai, Y., Miyamoto, K., Takenaka, H., and Yan, K. (2011) mTORC1 activation triggers the unfolded protein response in podocytes and leads to nephrotic syndrome. *Lab. Invest.* **91,** 1584–1595 CrossRef Medline
68. Delarue, F., Virone, A., Hagege, J., Lacave, R., Peraldi, M. N., Adida, C., Rondeau, E., Feunteun, J., and Sraer, J. D. (1991) Stable cell line of T-SV40

immortalized human glomerular visceral epithelial cells. *Kidney Int.* **40,** 906–912 CrossRef Medline

69. Mundel, P., Heid, H. W., Mundel, T. M., Krüger, M., Reiser, J., and Kriz, W. (1997) Synaptopodin: an actin-associated protein in telencephalic dendrites and renal podocytes. *J. Cell Biol.* **139,** 193–204 CrossRef Medline
70. Cheng, J., Wang, H., and Guggino, W. B. (2004) Modulation of mature cystic fibrosis transmembrane regulator protein by the PDZ domain protein CAL. *J. Biol. Chem.* **279,** 1892–1898 CrossRef Medline
71. Swiatecka-Urban, A., Brown, A., Moreau-Marquis, S., Renuka, J., Coutermarsh, B., Barnaby, R., Karlson, K. H., Flotte, T. R., Fukuda, M., Langford, G. M., and Stanton, B. A. (2005) The short apical membrane half-life of rescued uF508-CFTR results from accelerated endocytosis uF508-CFTR in polarized human airway epithelial cells. *J. Biol. Chem.* **280,** 36762–36772 CrossRef Medline
72. Huyer, G., Liu, S., Kelly, J., Moffat, J., Payette, P., Kennedy, B., Tsaprailis, G., Gresser, M. J., and Ramachandran, C. (1997) Mechanism of inhibition of protein-tyrosine phosphatases by vanadate and pervanadate. *J. Biol. Chem.* **272,** 843–851 CrossRef Medline
73. Liang, C. C., Park, A. Y., and Guan, J. L. (2007) *In vitro* scratch assay: a convenient and inexpensive method for analysis of cell migration *in vitro*. *Nat. Protoc.* **2,** 329–333 CrossRef Medline
74. Kimmel, C. B., Ballard, W. W., Kimmel, S. R., Ullmann, B., and Schilling, T. F. (1995) Stages of embryonic development of the zebrafish. *Dev. Dyn.* **203,** 253–310 CrossRef Medline
75. Schindelin, J., Arganda-Carreras, I., Frise, E., Kaynig, V., Longair, M., Pietzsch, T., Preibisch, S., Rueden, C., Saalfeld, S., Schmid, B., Tinevez, J. Y., White, D. J., Hartenstein, V., Eliceiri, K., Tomancak, P., and Cardona, A. (2012) Fiji: an open-source platform for biological-image analysis. *Nat. Methods* **9,** 676–682 CrossRef Medline